Journal of Inorganic Biochemistry 271 (2025) 112982

Contents lists available at ScienceDirect

Journal of Inorganic Biochemistry

journal homepage: www.elsevier.com/locate/jinorgbio

Near-infrared activation of upconversion platforms for non-redox-dependent release of Pt(II)

Marc-Ricard Batten [a], Josep Antoni Gutiérrez-Orgaz [a,b], Fernando Eduardo Maturi [c], Luís Dias Carlos [c], Helena Oliveira [d], Jordi Hernando [a], Fernando Novio [a], Antonio Rodríguez-Diéguez [e], Mercè Capdevila [a], Òscar Palacios [a], Pau Bayón [a,*]

[a] Chemistry Department, Faculty of Sciences, Universitat Autònoma de Barcelona, 08193-Cerdanyola del Vallès, Barcelona, Spain
[b] Institute of Chemical Research of Catalonia (ICIQ), Barcelona Institute of Science and Technology (BIST), 43007 Tarragona, Spain
[c] Phantom-g, CICECO–Aveiro Institute of Materials, Department of Physics, Universidade de Aveiro, 3810-193 Aveiro, Portugal
[d] Department of Biology and CESAM- Centre for Environmental and Marine Studies, University of Aveiro, 3810-193 Aveiro, Portugal
[e] Department of Inorganic Chemistry, Faculty of Science, University of Granada, Av/ Severo Ochoa s/n, 18071 Granada, Spain

ARTICLE INFO

Keywords:
Upconversion
Nanoparticles
Platinum
Release
cancer
Photoactivation

ABSTRACT

Upconversion nanoparticles (UCNPs) are a class of interesting nanomaterials with unique multi-photon excitation photoluminescence properties, and they have been intensively explored as novel contrast agents for biomedical imaging and drug delivery. The development of photoinduced drug-release devices has been intensively developed in the last years, specially using UCNPs due to their properties to absorb single-band near infrared (NIR) light and subsequently emit high-energy UV-to-visible light which could photoactivate several prodrugs. Some examples of Pt(II) release have been described, all of them from Pt(IV) complexes taking advantage of the Pt(IV)/(II) redox couple. In this work, NIR light-responsive $LiYF_4$:Yb/Tm UCNPs are presented as carrier systems to exert photoinduced Pt(II) drug release. For this, the surface of UCNPs were coated with an amphiphilic polymer to convert hydrophobic nanoparticles into hydrophilic and to load novel Pt(II) complexes. It is demonstrated that NIR radiation-induced Pt(II) drug release can be achieved without the need to use the Pt(IV)/(II) redox couple as a trigger. In this way, under NIR excitation, UCNPs can transform NIR irradiation into UV radiation which causes direct Pt(II) drug release in a spatial and temporal control manner. The release process has been monitored in real-time. Two platforms containing two different Pt(II) complexes have been studied, both showing similar results in terms of the enhancement of toxicity caused by the increase in Pt(II) concentration. Furthermore, a significant improvement of cytotoxicity against melanoma A375 cells was observed after irradiation of these platforms, confirming the feasibility of the proposed upconversion process to release Pt(II).

1. Introduction

Metals and metal complexes are of undeniable importance in therapies for multiple diseases [1]. In many cases, a limitation in these treatments is to control the spatial and temporal administration of the metal-based drugs. Over the years, examples have appeared where this control has been carried out by external stimuli through different strategies [2]. Among all of these, the use of electromagnetic radiation as an activator has been widely studied [3]. One of the main limitations in the use of radiation is the wavelength needed, that is, the energy implicit in that process. In many cases, the proposed photoactivatable systems required irradiation in the UV range, whereby the radiation itself causes damage to the cells and poorly penetrates tissues [4]. This is mainly due to the fact that UV-responsive metal complexes are more synthetically accessible, particularly through the design of ligands bearing simpler UV-absorbing motifs (*e.g.*, aromatics) [5]. Numerous efforts have been

Abbreviations: BSA, Bovine serum albumin; *ct*-DNA, Calf thymus DNA; DLS, Dynamic light scattering; EDX, Energy-dispersive X-ray spectroscopy; ESI-:MS, Electrospray ionization-mass spectrometry; FTIR, Fourier transform infrared spectroscopy; NIR, Near infrared; STEM, Scanning transmission electron microscopy; PBS, Phosphate-buffered saline; UCNPs, Upconversion nanoparticles; XRD, X-ray diffraction; XRPD, X-ray powder diffraction.

* Corresponding author.
E-mail address: pau.bayon@uab.cat (P. Bayón).

https://doi.org/10.1016/j.jinorgbio.2025.112982
Received 5 March 2025; Received in revised form 10 June 2025; Accepted 23 June 2025
Available online 24 June 2025

made in the last years to increase the activation wavelength to reach the less harmful visible range [6]. More recently, in very few examples, metal complexes capable of being activated with NIR wavelengths have been prepared [7], which not only further reduces the radiation energy but also provides a clear enhancement in penetration depth in tissues [8].

Solubility in biological media is another crucial issue in the rational design of photoresponsive species for the effective release of active metal complexes. In general, the increase in the activation wavelength, mentioned above, has been resolved by increasing the conjugation/electron delocalization in the metal ligands employed; however, this strategy usually leads to a decrease in solubility in aqueous media. This has become especially evident for Pt(II) [9].

Nanocarrier-based platinum drug delivery systems are promising alternatives to avoid the disadvantages of conventional platinum drugs such as reduced solubility, dose-limiting toxicity and different side effects [10]. Thus, drug carriers can afford photostability, water solubility, biocompatibility, and control of the cytotoxic effect for platinum complexes.

Specifically, platinum-loaded nanoparticles [11] ensure an increased blood circulation time and accumulation in tumor tissues through the enhanced permeation and retention (EPR) effect, resulting in improved therapeutic efficacy and reduced systemic toxicity [12].

A particular case in the use of platinum release mediated by nanoparticles has been UCNPs. In recent years, UCNPs have gained enormous interest for therapy and diagnostics, in particular, in controlled drug delivery [13]. The uniqueness of these nanoparticles of presenting anti-Stokes emission makes them especially attractive [14]. Through UCNPs it is possible to irradiate within the NIR biological window [15] (650–1300 nm) and generate UV–vis emission that could be used for the consequent activation of UV–vis responsive entities.

Conventional UCNPs for platinum delivery often rely on reduction of Pt(IV) to release cytotoxic Pt(II) species, with varying efficacy [16]. However, this work presents a distinct strategy. Herein, Pt(II) release is triggered by ligand modifications within the UCNP, achieving cytotoxicity without redox processes and enabling spatial-temporal control (Scheme 1). This approach deviates from existing UCNP-based Pt delivery methods.

Pt(IV) complexes have a huge potential as anticancer agents in terms of high activity and low toxicity, but this potential has been quietly exploited, because Pt(IV) is too easily reduced in the bloodstream [16a]. The potential advantages of Pt(IV) complexes remaining in the highest oxidation state in the bloodstream are that their lower reactivity would decrease the loss of active drug and reduce the incidence of unwanted side reactions leading to toxic side effects. Furthermore, the higher lipophilicity of some Pt(IV) complexes would be maintained, leading to potential improvements in cellular uptake.

However, all these advantages associated with Pt(IV), to a certain extent, cease to be so relevant when the platinum complexes are loaded into a vehicle such as UCNPs. Although in some cases the reduction of Pt(IV) to Pt(II) has been favored by UCNPs, in other cases this reduction has required external agents such as glutathione [16g,h,k]. All this casuistry made us consider the idea of directly using UV–vis photoreactive Pt(II) complexes and basing the release of Pt(II) on changes produced in the metal ligand, without the need of photoredox processes. Furthermore, if controlled Pt(II) release is achieved exclusively through the emission of the UCNPs, this would allow us to use Pt(II) complexes with UV–vis response. This is relevant since the design of a platform sensitive to NIR but with UV–vis active complexes would allow the recovery of many cytotoxic Pt(II) species that were no longer investigated given the high energy of the radiation necessary for their activation [3b].

In this work, we demonstrate the usefulness of UCNPs as activators of hydrophobic Pt(II) complexes in response to UV–vis radiation and how Pt(II) release can be done in a controlled manner within the NIR range. For this reason, two new complexes **C1** and **C2** have been designed, synthesized and characterized (Scheme 2) [17]. These complexes are endowed with photoactive nitrobenzene ligands (**L1** and **L2**, respectively) and can therefore act as photocages when irradiated with UV light. Therefore, in the design of the complexes, our starting hypothesis was that by photocleaving its nitrobenzene photocages, they should generate new Pt species that are reminiscent or even the same to those produced by the known drug oxaliplatin after aquation: analogs **C1'** and **C2'** after photocleavage of only one of the photocages, which could eventually transform into *cis*-[1,2-cyclohexanediamine-*N*,*N*']diaquo platinum (II) if a double cleavage occurred (Scheme 2).

2. Results and discussion

2.1. Synthesis of ligands L1 and L2 and complexes C1 and C2

Initially, the synthesis of ligand **L1** was undertaken. For this, α-nitrobenzaldehyde **1** was employed in the formation of diimine **3** with (±)-*trans*-cyclohexane-1,2-diamine, **2** (Scheme 3, Figs. S1–2). Subsequent double reduction of diimine **3** yielded ligand **L1** in 67 % yield (two steps). The ligand thus obtained was subsequently fully characterized (see experimental procedures and SI, Figs. S3–4). Once ligand **L1** was prepared, it was complexed with Pt(II). To obtain the corresponding dichloro Pt-complex, potassium tetrachloroplatinate was used as a platinum source. In this way, complex **C1** was finally obtained in 61 % yield. The complete characterization of **C1** (see experimental procedures and Figs. S5–6) revealed that the complexation occurred efficiently since the loss of symmetry of the starting ligand **L1** was observed by means of ^{1}H and ^{13}C NMR, which can be attributed to the fact that ligand **L1** adopts a non-symmetrical restricted conformation in the formation of **C1**. Also, a peak detected by MS ([M^{+}+DMSO-Cl^{-}] = 813.1703 Da, calc. = 813.2030 Da), showing the characteristic platinum pattern,

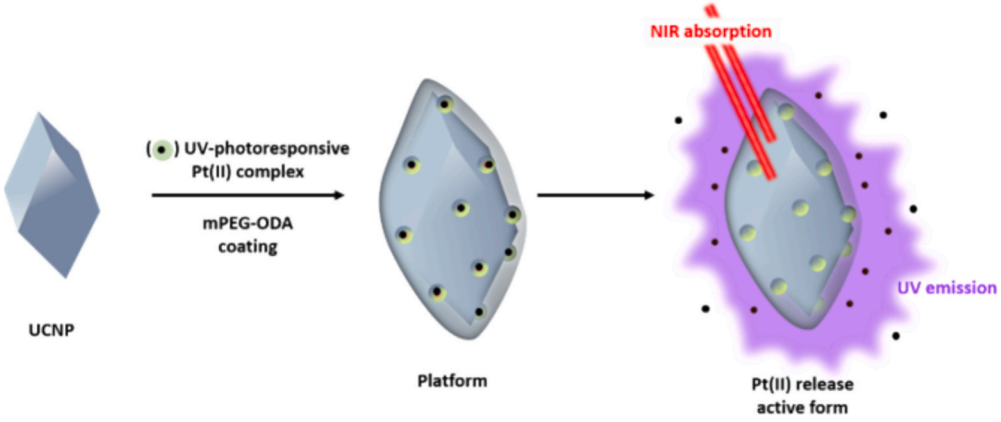

Scheme 1. NIR-activated release of Pt(II) by means of UCNP-based carrier platform. Figures in this scheme are original and created by the authors.

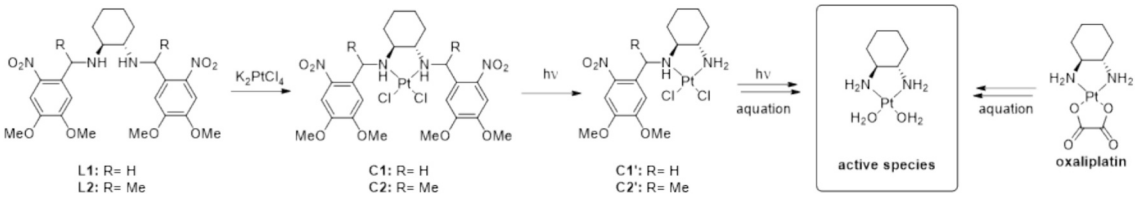

Scheme 2. Synthesis and expected photouncaging of complexes **C1** or **C2** and subsequent aquation to give analog species to those obtained from oxaliplatin.

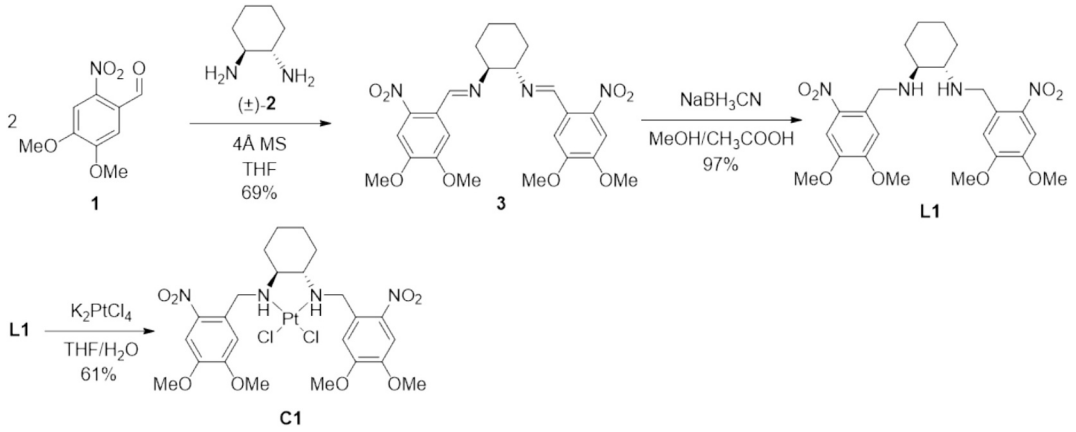

Scheme 3. Synthesis of ligand **L1** and complex **C1**.

could be attributed to complex **C1** (Fig. S7).

The synthesis of the **L2** ligand proved to be much more challenging. The synthesis for **L2** was initially proposed analogously to that of **L1** (Scheme 4a). Therefore, a strategy based on a reductive amination was again chosen, starting from 4,5-dimethoxy-2-nitroacetophenone, **4**. However, formation of the corresponding diimine could not be achieved in synthetically useful yield. Different attempts were made at different conditions involving solvent and temperature. Also, microwave-assisted tries were performed. In all cases, an equilibrium between racemic diamine **2** and the corresponding monoamine **5** was reached, and no diamine was detected. Because of this, reductive amination starting from acetophenone **4** and diamine (±)-**2** was performed one-pot in the presence of titanium isopropoxide in combination with $NaBH_4$ following a previously described procedure (Scheme 4b) [18]. Under these conditions, a useless mixture of starting ketone **4** together with different products was obtained. This lack of reactivity was attributed to the nitro group in ortho-benzyl position in **4**. Thus, the reaction was repeated starting from 1-(3,4-dimethoxyphenyl)ethan-1-one, **6**. In this way, the diamine ligand **7** was isolated in a 99 % yield but, disappointingly, as an inseparable diastereomeric mixture (Fig. S8).

Alternatively, the double methylation reaction of diimine **3** was considered since it would be convenient to use a common intermediate in the synthesis of both **L1** and **L2** ligands. However, despite multiple attempts with different nucleophiles (MeMgBr [19] or MeLi [20]), neither the mono- nor the di-addition of methyl group was likely in any case probably due to the presence of nitro groups [21]. These results

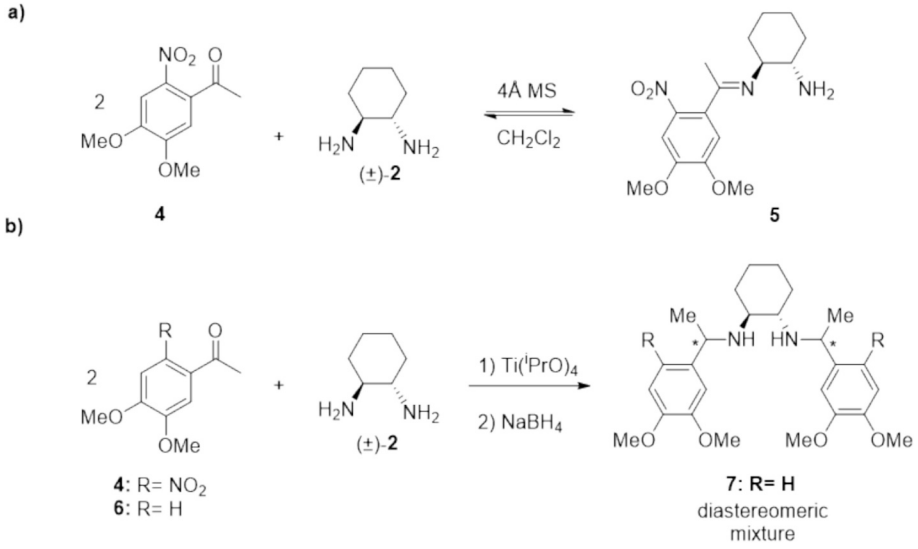

Scheme 4. a) Attempt to synthesize ligand **L2** starting from 4,5-dimethoxy-2-nitroacetophenone, **4**. b) Attempts of one-pot synthesis of ligand **L2** in the presence of $Ti(^iPrO)_4$ followed by $NaBH_4$ reduction.

prompted us to explore a new synthetic approach for **L2**. Thus, a new route avoiding nitro groups until the end of the synthesis was proposed starting from 3,4-dimethoxybenzaldehyde, **8**, and racemic diamine **2** (Scheme 5).

In this way, the corresponding diimine **9** was obtained in a satisfyingly 76 % yield [22]. As expected, diimine **9** turned out to be a better electrophile than **3** and double methylation was finally achieved in 90 % yield using MeLi as the nucleophile. To our delight, in this case, diamine **7** was obtained with complete diastereoselectivity as revealed by ^{1}H and ^{13}C NMR analysis showing a single set of signals (Figs. S9–10). Diamine **7** was next subjected to double nitration under standard conditions. Finally, ligand **L2** was thus obtained in 62 % yield from **8** as a single diastereomer and was fully characterized (see experimental procedures and SI, Figs. S11–12). Eventually, crystallization of a nitrate salt of **L2** from EtAcO/^{i}PrOH provided cube-shaped crystals suitable for X-ray analysis (Fig. 1), which show the relative configuration of the four stereogenic centers.

The formation of the Pt(II) complex **C2** was carried out under analogous conditions than for **C1**. In this way, ligand **L2** was complexed to form **C2** in 28 % yield. Complex **C2** was then fully characterized and analogously to **L1** and **C1**, the loss of symmetry upon complexation was corroborated by NMR (Figs. S13–14). Finally, mass spectrometry showed a clear peak attributed to complex **C2** ([M^{+}+Na^{+}] = 821.1461 Da, calc. = 821.5678 Da) with characteristic platinum pattern (Fig. S15).

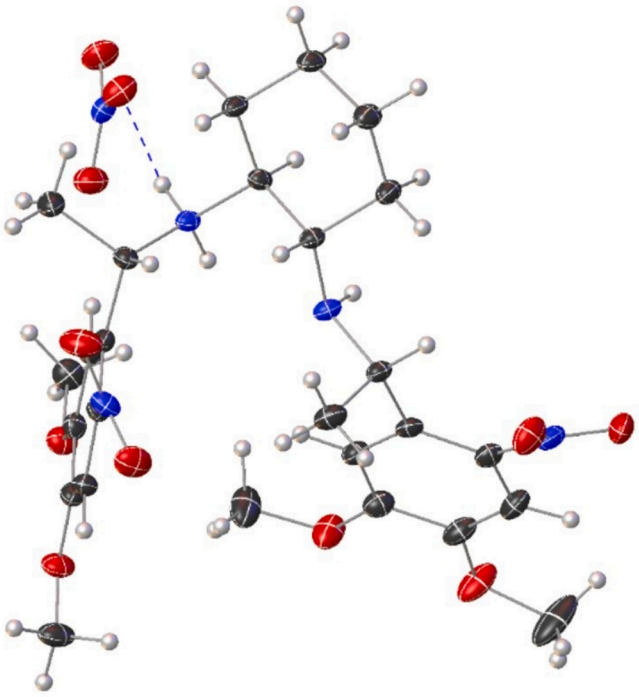

Fig. 1. ORTEP representation for the resolved structure of ligand **L2**·HNO_3. Color code: carbon atoms in grey, nitrogen in blue, oxygen in red and hydrogen in light grey. Hydrogen bond shown in blue dash line. (For interpretation of the references to color in this figure legend, the reader is referred to the web version of this article.)

2.2. Synthesis and characterization of UCNPs

The synthesis of oleate-coated UCNP $LiYF_4$, doped with Yb^{3+} (25 %) and Tm^{3+} (0.5 %) ions, was based on a procedure already described (Scheme 6) [23].

It is well known that the rhombohedral morphology of these UCNPs is crucial for their optical properties [24]. However, despite following the described protocols, the results in terms of morphology and consequently, optical properties of different attempts were not consistent. In some cases, UCNPs appeared as spheres and in others as rhomboids, without apparently any correlation with the conditions employed. As small variations have important influence in the size and shape or the UCNPs [25], a consistent protocol for their preparation was established. The first synthetic step was common to all the studies (Scheme 6). It

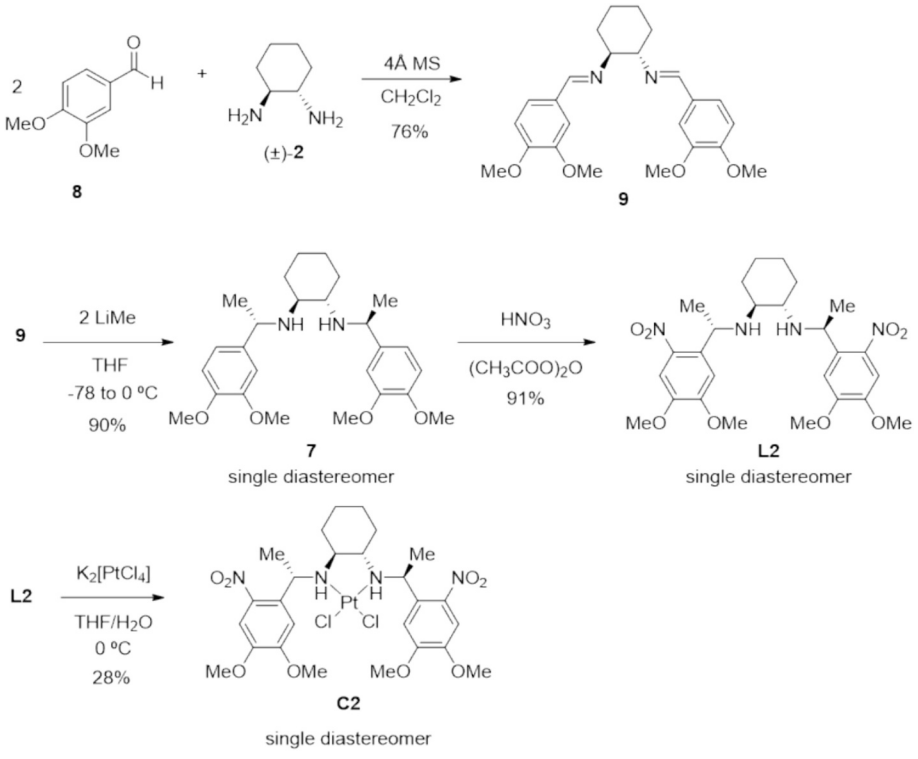

Scheme 5. Synthesis of ligand **L2** from 3,4-dimethoxybenzaldehyde, **8**.

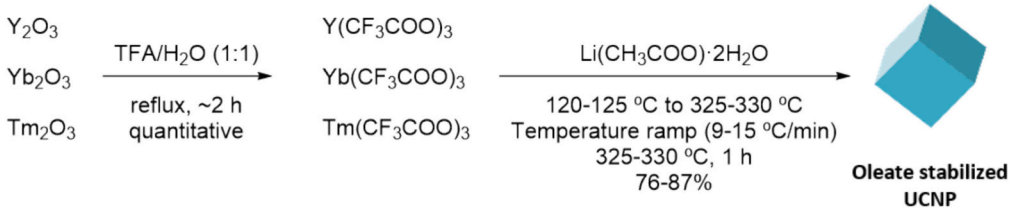

Scheme 6. General procedure for the synthesis of UCNPs.

consisted in the formation of the yttrium and lanthanide trifluoroacetate precursors, $M(CF_3COO)_3$ (M: Y, Yb and Tm), by heating a mixture of oxides (Y_2O_3:Yb_2O_3:Tm_2O_3) at a given molar ratio in aqueous TFA (1:1) (see experimental section). In this way, a $M(CF_3COO)_3$ mixture was quantitatively isolated as a white powder. Next, the $M(CF_3COO)_3$ precursors were thermally decomposed in the presence of Li^+. Although the use of 2 eq. of LiF [26], 1 eq. of $Li(CF_3COO)$ [23] or 1 eq. of $LiAcO{\cdot}2H_2O$ [27] has been reported, after some screening, $LiAcO{\cdot}2H_2O$ was chosen as the appropriate lithium source. Thus, several thermal decompositions were then performed at different temperature ramps with 1 or 2 equivalents of $LiAcO{\cdot}2H_2O$, to find the optimal conditions for nanoparticle synthesis (Table 1 and Fig. 2a).

Following a general procedure, a $M(CF_3COO)_3$ mixture with 1 or 2 equivalents of $LiAcO{\cdot}2H_2O$, was heated in the presence of oleic acid and 1-octadecene (1:1 ratio). For this, the mixture was first degassed at 120–125 °C and then heated to high temperatures at different rates under N_2 (Fig. 2a). In all cases, the mixture was maintained at the final temperature for 1 h. After cooling to RT, non-polar oleate-capped UCNPs were precipitated by the addition of absolute ethanol to the reaction mixture. Then, the precipitates were isolated by centrifugation and subsequently washed to obtain UCNPs as greyish-white solids in 80 % average overall yields. The morphology and composition of the nanoparticles obtained in each test was checked by scanning transmission electron microscopy (STEM), Fig. 2b, the elemental mapping was analyzed by energy-dispersive X-ray spectroscopy (EDX), Fig. S16, and the phase identification by X-ray powder diffraction (XRPD), Fig. S17. From these results, the best conditions were stablished as: 2 eq. of $LiAcO{\cdot}2H_2O$ and the final temperature reached as 330 °C with a ramp of 15 °C/min (Sample IIIb). In this way, homogeneous and well-defined rhombohedral UCPNs were consistently obtained.

Once a reliable procedure for the preparation of rhombohedral UCNPs was established, it was investigated whether their shape influenced their optical response when measured as solid powders and under irradiation with NIR radiation. Comparing the emission spectra of spherical and rhombohedral UCNPs, the morphology revealed indeed crucial. Thus, while the same upconversion emission bands arising from different thulium transitions were measured in both cases, it was observed that rhombohedral UCNPs exhibited more intense luminescence under equivalent photoexcitation conditions (Fig. 3). For these UCNPs, the quantum yield of the upconversion process was measured to be 0.053 % when irradiated at a power of 580 W/cm^2. As already reported for similar UCNPs [28], the upconversion emission of the nanoparticles synthesized herein spans over a large spectral range and, more importantly, it allows the generation of UV luminescence photons under excitation with NIR radiation, as required for our purposes.

Table 1
Representative reaction conditions and yields in the second step for the UCNPs synthesis. All samples were kept at the final temperature for 1 h.

Sample	Ramp T (°C/min)	Li(AcO)·2H$_2$O (eq.)	Final T (°C)	Yield (%)[a]
I	9	1	315	70
II	11	1	325	80
IIIa	15	1	325	87
IIIb	15	2	330	76

(a) Indicative yields since the composition/coating of each batch may vary slightly.

With complexes **C1** and **C2** and UCNPs in hand, the next step was to coat the nanoparticles with a polymer able to embed and retain the platinum complexes. For this, a previously described methodology was applied in which the amphiphilic polymer methoxy poly(ethylene glycol)-octadecylamine (mPEG-ODA) [29] was used as the coating agent [26]. Basically, the corresponding platinum complex, the UCNPs and mPEG-ODA were dispersed in a mixture of water and chloroform (see experimental section). Specifically, in the case of **C1**, it was necessary to add THF to increase the solubility of the Pt(II) complex. The resulting suspensions were stirred vigorously, and the organic solvent was slowly evaporated at 45 °C. After this process, the coated nanoparticles together with an excess of mPEG-ODA were isolated. The excess coating polymer was removed by redispersion in water and filtration through a 0.4 μm pore size filter [30]. Finally, **C1** and **C2**-mPEG-ODA-coated nanoparticles (platforms **P1** and **P2**) were lyophilized. Removal of water under vacuum at 60 °C was also tried, but part of the nanoparticles was disaggregated or degraded as observed by STEM.

Platforms **P1** and **P2** were characterized by different techniques: STEM, EDX, dynamic light scattering (DLS), Fourier transform infrared spectroscopy (FTIR) (Figs. S18–21), ζ-potential measurements and inductively coupled plasma optical emission spectroscopy (ICP-OES). The stability of the platforms was also verified. To this aim, it was first observed by DLS analysis that the UCNPs were stable after one week in water, phosphate-buffered saline (PBS), and PBS + bovine serum albumin (BSA). Similarly, it was confirmed that **P1** and **P2** also remained unchanged after one week in water (Fig. S20). FTIR study determined that UCNPs had been successfully coated with PEG-ODA polymer in both cases (**P1**, **P2**). The low concentration of Pt compared to the polymeric material did not allow the detection of such complexes by this technique due to the shielding of the polymer signals (Fig. S21). STEM showed a 4 nm thin layer surrounding the nanoparticles, demonstrating that the UCNPs were coated (Scheme 7). This coating seems to produce slight changes in their morphology, as they showed more ellipsoid than rhombohedral shapes (Scheme 7).

The presence of the Pt(II) complex loaded on mPEG-UCNPs through the lipophilic interaction in platforms **P1** and **P2** was confirmed by EDX as, in comparison with starting UCNPs, new peaks corresponding to Pt were detected (Figs. S17–18). The Pt(II) loading for these platforms was determined through ICP-OES resulting in 1.0 % and 1.8 %, for **P1** and **P2** respectively [31]. Also, a size around 120 nm was determined by DLS for **P1** and **P2** (Fig. S19). In addition, a ζ-potential of −12 mV was determined for these materials, thus indicating that the carbonyl groups in mPEG-ODA are majorly pointing toward the outside of the platform and consequently, the amide nitrogen atoms are toward the inside of the platforms [32].

2.3. Photochemical characterization of ligands and complexes

The photoactive behavior of ligands **L1** and **L2**, as well as that of their corresponding complexes **C1** and **C2**, was investigated. Initially, the UV–vis absorption spectra of the ligands were recorded and compared with those of their corresponding complexes (Fig. 4). Both **L1** and **L2** ligands presented absorption bands peaking at λ_{abs} = 242/245, 292/305, and 344/345 nm, respectively, which were attributed to their

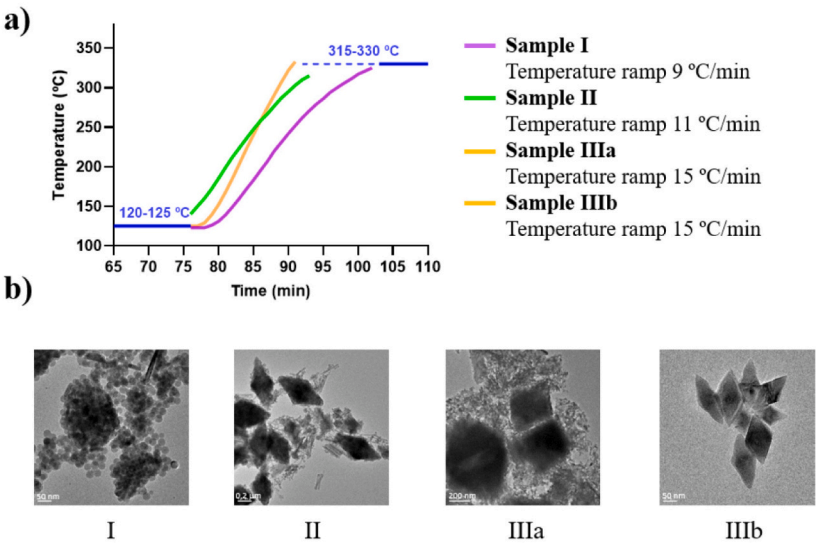

Fig. 2. a) Plot of the different temperature ramps used in the thermal decomposition/morphology study. b) STEM images of the corresponding UCNPs obtained for each ramp.

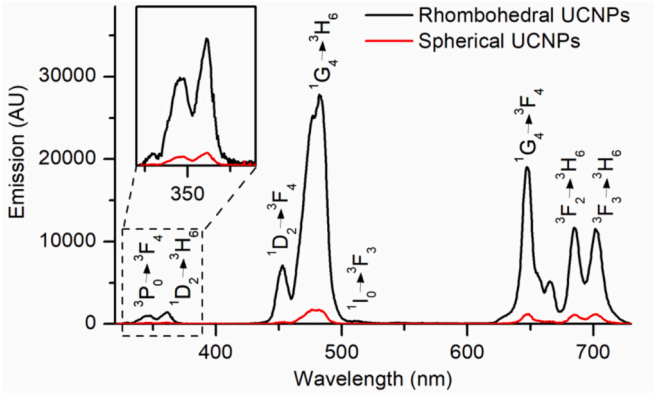

Fig. 3. Emission spectra of spherical and rhombohedral UCNPs measured as solid powders under NIR irradiation (λ_{exc} = 980 nm, power density = 3.8 W/cm^2, $\lambda_{detection}$ = 320–730 nm). The thulium emission transitions are indicated in the figure.

nitroaromatic chromophore. Upon Pt(II) complexation, the band around λ_{abs} ~ 300 nm decreased in intensity, while the others only suffered minor spectral shifts. As a result, both **C1** and **C2** presented large absorption within 330–400 nm spectral range, which nicely overlaps with the UV emission of UCNPs (Fig. 3).

o-Nitrobenzyl derivatives undergo the UV-induced release of the leaving group installed at the benzylic position through an intramolecular rearrangement reaction that produces the corresponding *o*-nitrosobenzaldehyde or *o*-nitrosobenzophenone as by-products [33]. To investigate this process for **L1**, **L2**, **C1**, and **C2**, first, the variation of their steady-state electronic absorption spectra upon irradiation with 365 nm UV light in acetonitrile was monitored (Fig. 5). For ligand **L1**, different spectral changes were observed in this experiment: an increase in the intensity of the band at ~242 nm, the emergence of a new band at ~275 nm, and the rise and red-shifting of the band at ~344 nm which eventually decreases in intensity upon further irradiation. The latter suggests the existence of at least one intermediate species during the photoreaction of **L1** under UV irradiation. Interestingly, this outcome was not observed for **L2**. Instead, only the initial increase and bathochromic shift of the absorption band at ~345 nm was observed in this case. In contrast, the behavior of complexes **C1** and **C2** was found to be much more similar, as both were characterized by the increase and red-shift of the absorption band at ~350 nm as well as the appearance of a new band at ~520 nm and 496 nm, respectively. Remarkably, for **L2** and **C2**, isosbestic points were observed during the UV-induced evolution of their UV–vis absorption spectra, which suggested the involvement of only two species in their photoreaction process. For all four investigated compounds, the mixtures obtained after irradiation appeared to be stable in the dark for several days, especially if kept at low temperature. In addition, no subsequent recovery of the starting spectra in the dark was observed, confirming that all the ligands and complexes undergo irreversible phototransformation.

Under equivalent UV irradiation conditions, the spectral changes occurring for **L1** and **L2** were found to be faster than for the

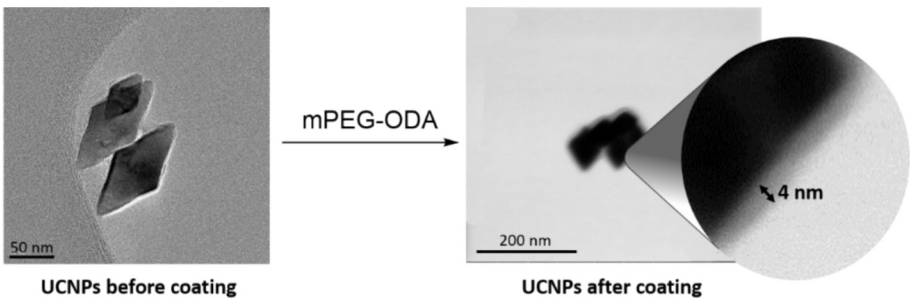

Scheme 7. STEM images of the rhombohedral UCNPs before and after mPEG-ODA coating for the determination of the thickness of coating.

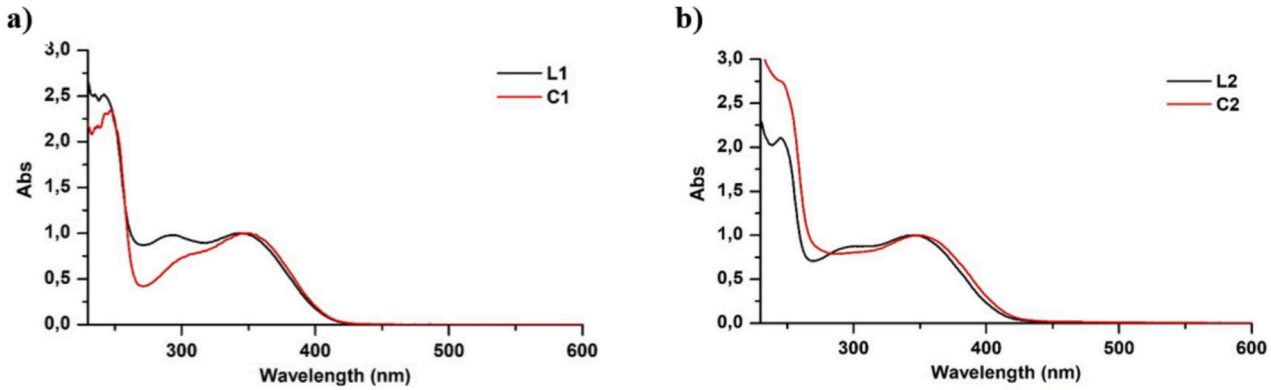

Fig. 4. Comparison of UV–vis absorption spectra in CH_3CN, before and after complexation for a) **L1** and **C1** and b) **L2** and **C2**. In all cases, the spectral maximum of the absorbance band around 350 nm has been normalized to 1 for comparison purposes.

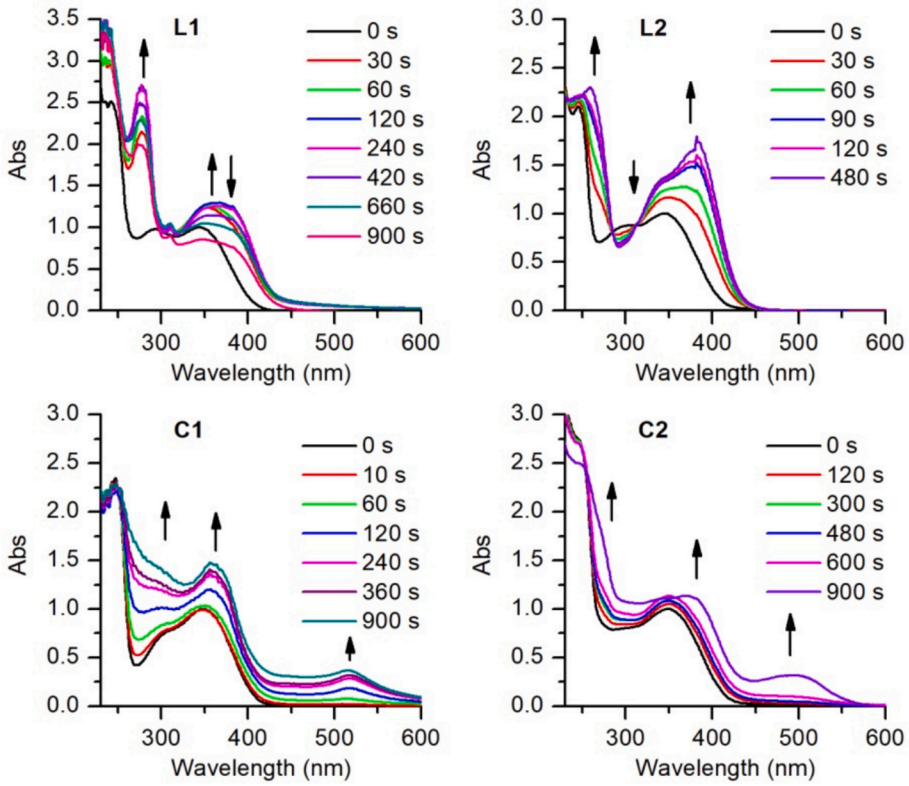

Fig. 5. Time evolution of the UV–vis absorption spectra of ligands **L1** and **L2**, and their Pt(II) complexes **C1** and **C2** upon UV irradiation in CH_3CN solution (365 nm and power density of 3 mW/cm^2 at 1.0 × 10^{-5} M). In all cases, the maximum of the absorbance band around 350 nm for the initial spectrum (t = 0 s) has been normalized to 1 for comparison purposes.

corresponding complexes **C1** and **C2**. To rationalize this behavior, the quantum yields of their photoreactions (Φ_{ph}) in acetonitrile were determined by analyzing the time dependence of their absorption variation at 355 nm relative to a reference (1, 2-bis(2-methyl-5-trifluoroacylthien-3-yl)cyclopentene, $\Phi_{o\text{-}c}$ = 0.37 in toluene [34]). In the case of **L1**, whose photodegradation process presents two distinguishable steps, the quantum yield was determined only for the first of them. As expected, higher Φ_{ph} values were measured for the ligands that agree with the data reported for other *o*-nitrobenzyl photoremovable groups [33]: Φ_{ph} = 0.406 and 0.147 for **L1** and **L2**, with the corresponding Φ_{ph} ε_{abs} factors characterizing the efficiency of the photoreaction being 10,041 and 7424.3 $M^{-1}{\cdot}cm^{-1}$, respectively. Complexation to Pt(II) complexes detrimentally affected the efficacy of the photoreactions, as lower Φ_{ph} and Φ_{ph} ε_{abs} values were determined for **C1** (Φ_{ph} = 0.015 and Φ_{ph} ε_{abs} = 150 $M^{-1}{\cdot}cm^{-1}$) and **C2** (Φ_{ph} = 0.028 and Φ_{ph} ε_{abs} = 224 $M^{-1}{\cdot}cm^{-1}$). Because of the similarity of the ligands and complexes absorption spectra, the decrease of the photoreaction quantum yield observed for the complexes relative to the free ligands should be ascribed to the emergence of new relaxation pathways for the intraligand excited state generated in the complexes upon irradiation at 365 nm. For instance, this could be the case of photoinduced electron transfer from the ligand-centered singlet excited state to the Pt center. Despite this, the Φ_{ph} ε_{abs} factors obtained for the complexes are still sufficiently large to allow photoreaction to take place at reasonable rates.

To further investigate the UV-induced photoreactions of **L1** and **L2** as well as **C1** and **C2**, they were monitored by ^{1}H NMR, electrospray ionization-mass spectrometry (ESI-MS) and X-ray diffraction (XRD). In

the case of **L1**, a similar behavior to that observed by UV–vis absorption spectroscopy was registered. At short irradiation times in acetonitrile-d_3, the formation of an initial product was observed and characterized by a ^{1}H NMR singlet at $\delta = 12.10$ ppm and some peaks in the aromatic region (Fig. 6, $t = 35$ min).

This spectral pattern is compatible with the generation of the expected *o*-nitrosobenzaldehyde by-product **10** ([M + H$^+$] = 196.0607 Da, calc. = 196.0610 Da, Fig. S22) accompanied by the release of diamine **L1'** (Scheme 8a). Indeed, the presence of **L1'** in the mixture, produced at short irradiation times, was corroborated by mass spectrometry. However, this product was not stable upon further irradiation, as it totally evolved to the formation of a unique stable photoproduct as recorded by ^{1}H NMR (Fig. 6, $t = 114$ min). To obtain more information and to identify this photoproduct, a sample was crystallized, and its structure was finally resolved as 1*H*-pyrazole **11** (Scheme 8 and Fig. S23). Formation of this tricyclic compound was attributed to a Davis-Beirut-type [35] reaction of the enamine resulting from aldehyde **10** and amine **L1'** which indicates that only one photodeprotection reaction takes place within **L1** bearing two amino groups protected with *o*-nitrobenzyl moieties. The formation of **11** was also confirmed by mass spectrometry analysis of the same sample ([M + H$^+$] = 469.2088 Da, calc. = 469.2087 Da), Fig. S24).

Interestingly, the photodegradation of the corresponding complex **C1** lead to complex **C1'** appearing to be stable after 3 h of continuous irradiation together with the nitroso aldehyde **10** (Scheme 8a). The presence of **C1'** was corroborated by mass spectrometry ([M + Na$^+$] = 598.1 Da, calc. = 598.3 Da, Fig. S25).

The photodegradation of ligand **L2** and complex **C2**, after 1 h of irradiation for **L2** and 2 h for **C2**, showed in both cases the formation of stable species (Scheme 8b). These photoproducts were attributed to the nitroso ketone **12** ([M + H$^+$] = 210.0756 Da, calc. = 210.0766 Da) and diamine **L2'** ([M + H$^+$] = 324.1927 Da, calc. = 324.4010 Da) or the corresponding complex **C2'** ([M-Cl$^-$ + H$^+$] = 554.1158 Da, calc. = 554.1260 Da) when starting from **L2** or **C2**, respectively (Figs. S26–27).

2.4. Photoinduced Pt(II) release from P1 and P2

Once proven the photoreactivity of **C1** and **C2** under direct UV irradiation, the main concern was to verify if the same process could be induced by UCNPs when these complexes were loaded on the coating layer of the **P1** and **P2** platforms and, as a result, an increased release of Pt(II) could be triggered under illumination. For this purpose, three different experiments for each platform were carried out in PBS solution at 37 °C. As a control experiment, one test consisted of monitoring the Pt (II) release while keeping the platforms in the dark. A second test consisted of monitoring the Pt(II) release while irradiating within the UV range (365 nm), and the third test was carried out under NIR irradiation (980 nm). All the tests were performed in duplicate. The Pt(II) content in the initial sample and the amount of released Pt(II) species at different times were determined using ICP-OES. Fig. 7 shows the Pt(II) release curves *versus* time for platforms **P1** and **P2** under the three different conditions (Table S1).

Both plots show Pt(II) released from both platforms in absence of light (after 24 h, up to 45 % for **P1** and less than 40 % for **P2**). This release could be attributed to a direct diffusion of the entrapped complexes. However, in the presence of NIR and UV radiation, there was a much higher % release of Pt(II) yet in less time (70–80 % for **P1** and 60–70 % for **P2**).

Since it was not possible to detect the form in which Pt(II) is released with ICP-OES, experiments were performed to try to identify the released species. To do this, the supernatant content of three suspensions of the **P2** platform in water was analyzed by HPLC after being submitted to irradiation or dark conditions at room temperature. While one of the suspensions was left in the dark, the other two were irradiated under UV (365 nm) or NIR (980 nm) at room temperature. The samples were then ultracentrifuged and the supernatants were analyzed by HPLC. The analysis of the supernatant corresponding to the sample in the dark

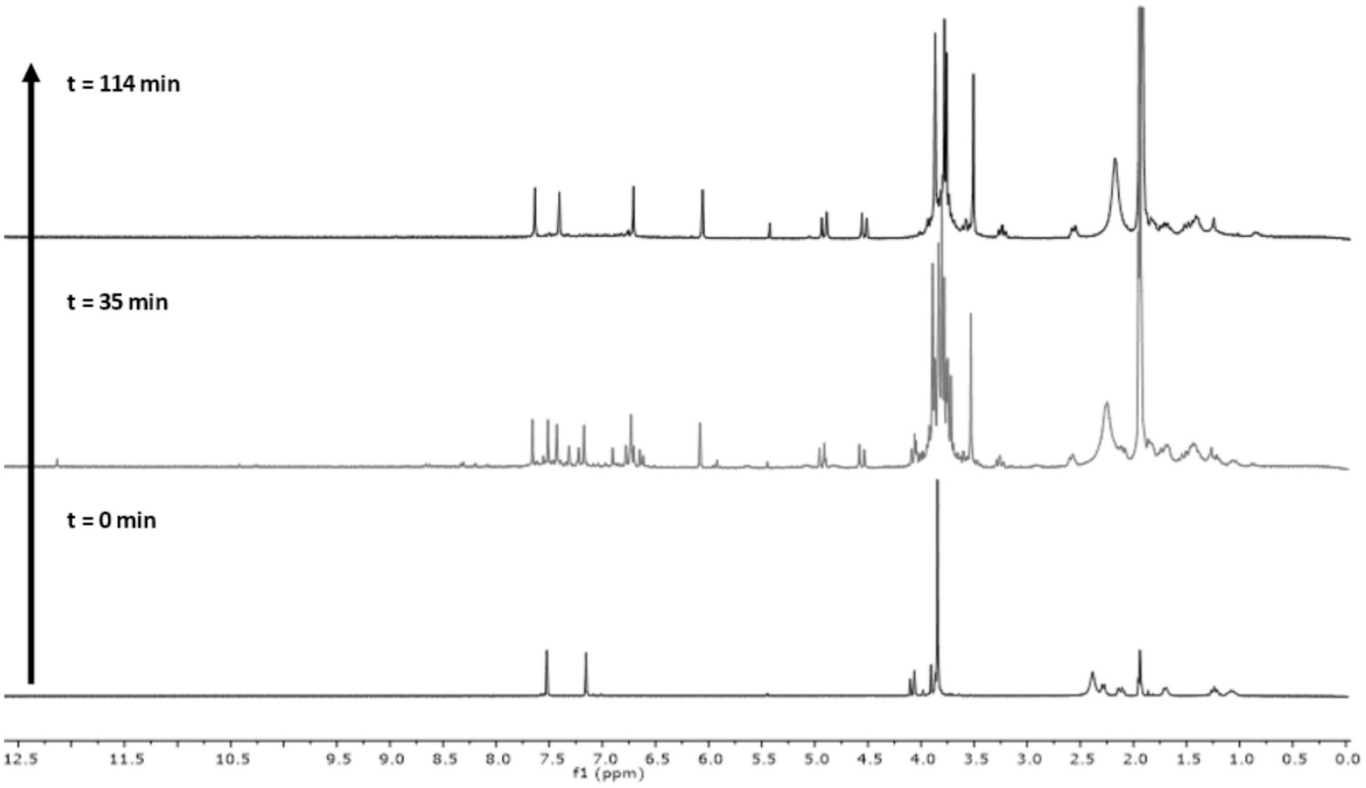

Fig. 6. 400 MHz ^{1}H NMR spectra (acetonitrile-d_3) of the photodegradation of **L1** at 365 nm.

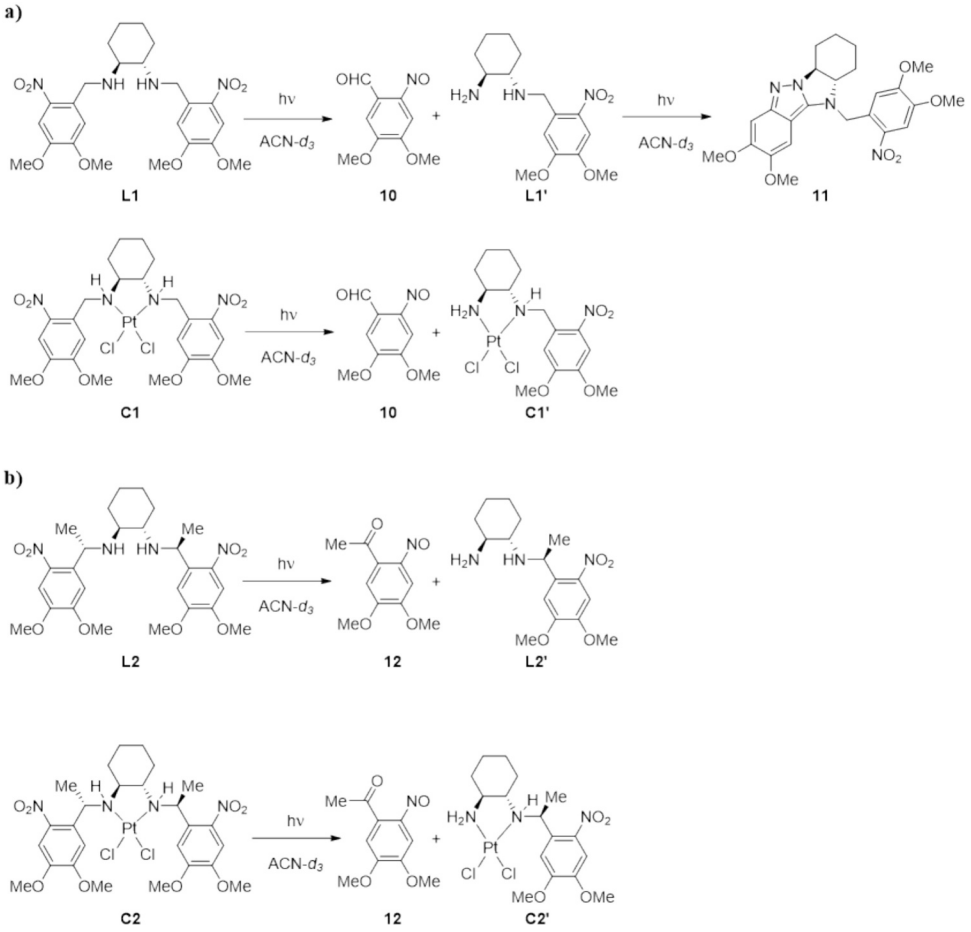

Scheme 8. Photoreactions under irradiation at 365 nm of a) **L1** and **C1** and b) **L2** and **C2**.

(Fig. S29a), mainly showed a peak at rt. = 9.4 min corresponding to the **C2** complex (by comparison with a sample of the pure complex, Fig. S30) together with another peak at rt. = 9.9 min. This additional peak was attributed to a species derived from **C2**, probably through a chloride/aquo complex exchange, since its intensity was found to increase at the expense of the peak corresponding to **C2** when incubating a **P2** sample in water for 24 h in the dark (Fig. S31). For both peaks, the UV spectrum was analyzed and resulted in very similar profiles ($\lambda_{abs,max} \sim 350$ nm), which confirmed that they were structurally similar species. Interestingly, no relevant peak attributable to the free ligand was observed (by comparison with the HPLC chromatogram of pure ligand **L2**, Fig. S32). The supernatant of the UV irradiated sample (Fig. S29b) showed a chromatogram where an almost complete conversion into a new species was observed with a UV spectrum similar to that of **C2** but with a very different retention time (rt = 6.3 min). Therefore, this peak was attributed to the **C2'** photoproduct. Also, according to the release curve (Fig. 7) it would be expected that in this chromatogram also **C2** or even **L2** would be observed. However, this was not the case. This could be because under irradiation, the possible released **C2** complex would be also photodegraded in the suspension medium itself. As for the supernatant subjected to NIR irradiation (Fig. S29c), its HPLC chromatogram showed both the peaks attributed to **C2** and its degradation product in the dark (rt = 9.4 and 9.9 min), which would be consistent with the non-selective release of a portion of **C2**. More interestingly, a clear increase in the signal corresponding to the desired **C2'** photodegradation product also observed with direct UV irradiation was found (rt = 3.3 min). This fact shows how the photodegradation of **C2** and, therefore, the corresponding release of **C2'** is triggered by irradiating in the NIR, as devised in our design.

From the combination of ICP-OES HPLC results, using **C2** as a model, it would seem reasonable to think that the increase in Pt(II) release measured under irradiation is enhanced by the light-induced formation of the **C1'** and **C2'** photoproducts. Although this release mechanism is not selective and competitive diffusion of intact **C1** and **C2** complexes is also observed, our photorelease experiments validate the initial hypothesis of the present work – *i.e.*, the capacity of using the UV upconversion emission of UCNPs generated *in situ* under NIR irradiation to produce Pt(II) release from the surrounding coating layer by ligand photouncaging. As a result, after about 400 and 200 min of NIR irradiation of **P1** and **P2**, respectively, efficient light-induced Pt(II) release is achieved, noticeably higher than in the dark.

2.5. Biological assessment of ligands, complexes and their photoproducts

Since DNA is the targeted biological entity, the *in vitro* reactivity of the single complexes **C1** and **C2** and their photoproducts toward DNA was investigated under different conditions. This reactivity was followed by circular dichroism (CD) and UV–vis absorbance spectroscopies.

Circular dichroism. First, the interaction of complexes **C1** and **C2** and the corresponding photoproducts **C1'** and **C2'** with DNA was assessed by CD. CD is a technique that is highly sensitive to any small change in the structure of the DNA [37] and is widely used to study the interaction between metal-complexes and DNA [38]. It is well known that when Pt(II) compounds bind to DNA they can provoke structural changes in the nucleic acid, impairing the replication of the cells, thus acting as cytotoxic agents. DNA presents two bands in the CD spectra at the UV region: base stacking causes a positive band at 275 nm, while a

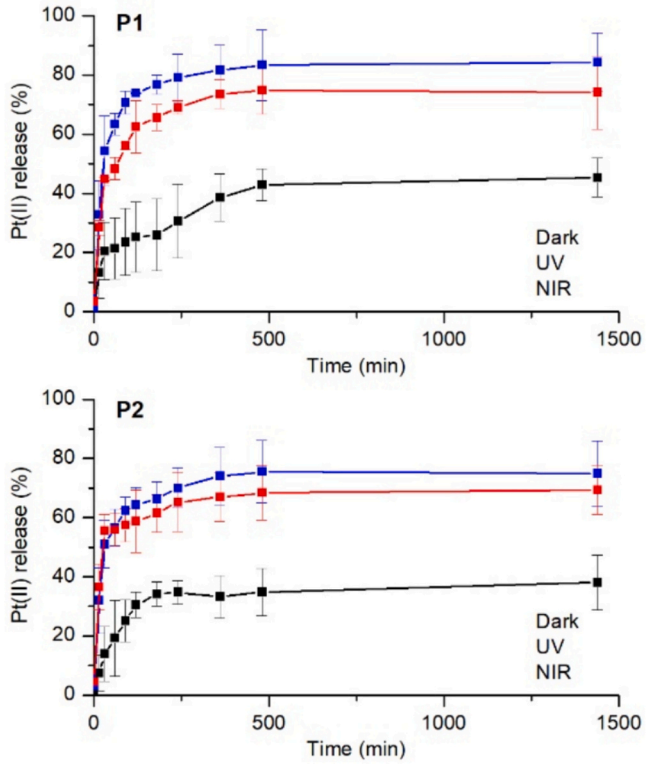

Fig. 7. Pt(II) release profiles for platforms **P1** and **P2** in the dark and under 365 nm UV, and 980 nm NIR irradiation. In all cases, average data for two independent tests are plotted ($n = 2$) and errors bars are given as the standard error of the mean.

negative band at 245 nm is caused by the right-handed helicity of β-DNA [39].

In this case, to investigate if the Pt(II) species can interact and perturb the DNA strands, replicates of a 50 μM calf thymus DNA (*ct*-DNA) solution were incubated with each of the complexes at different molar ratio ($r = 0$ to 2) along 24 h at 37 °C (Fig. 8).

The CD data showed minor interactions between *ct*-DNA and the complexes, in their forms before and after irradiation. For the non-irradiated Pt(II) complexes **C1** and **C2** there is an increase in both, the positive and negative bands, presenting **C1** a large bathochromic shift. Besides, the CD spectra of the photoproducts **C1'** and **C2'** also show an increase and a bathochromic shift for the 245 nm band, but the band at 275 nm decreases with a bathochromic shift in both cases. These results indicate that Pt(II) complexes before and after being irradiated bind to DNA, destabilizing both the base stacking and helicity.

Electronic absorption spectroscopy. The interaction of the complexes with *ct*-DNA was also detected by UV–vis absorption spectroscopy. Unlike those previous CD experiments, in this study the concentration of the Pt(II) complexes was constant, while the DNA concentration gradually increased. If the reaction is highly selective and specific or poorly reactive, the signals associated with the complex would gradually decrease with each addition of DNA. Instead, if the reaction is non-specific, fast, and/or strong, the signal of the complex would disappear from the first addition. In either case, the binding constant can be estimated by the Benesi-Hildebrand approach [40].

The absorbance of each compound alone was recorded at 50 μM and as *ct*-DNA (0–100 μM) was added, the changes in absorbance were monitored (Fig. S33). All compounds showed a hypochromic effect as the concentration of *ct*-DNA increased and no significant bathochromism was observed in any spectra. This suggests an interaction in all cases with DNA *via* groove binding or electrostatic interactions rather than *via* intercalation with π orbitals of the DNA base pairs [41]. Changes in UV spectra revealed specific for each compound. While for **C1'** and **C2** the variation was slight, with a gradual decrease of the signal, for **C1** and **C2'** the variations were more pronounced.

The nature of the interaction of the complexes with DNA was further investigated. The intrinsic binding constants (K_b) were calculated using the Benesi-Hildebrand host-guest equation [41a,c]. High K_b values are usually attributed to strong intercalation with the DNA bases, while low K_b values denote poor intercalation of the complex. Table 2 shows the

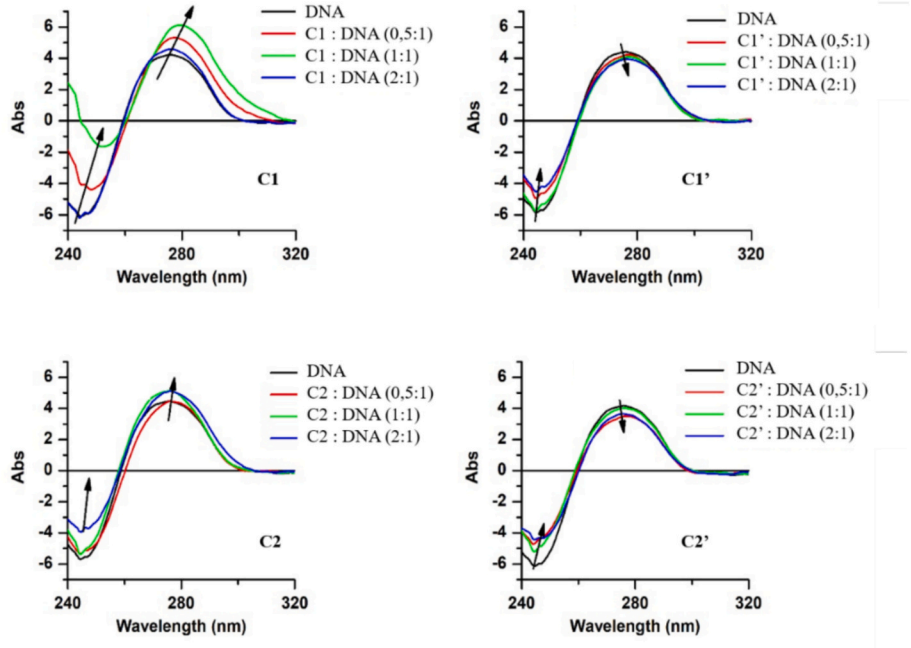

Fig. 8. CD spectra recorded for the incubation of *ct*-DNA with **C1, C1', C2** and **C2'** at [0.5:1], [1:1] and [2:1] [Complex:DNA] molar ratios in Tris·HCl, at pH 7.2. All samples were incubated at 37 °C for 24 h.

values obtained for **C1** and **C2** and their corresponding photoproducts.

The range of K_b values between 1.8×10^3 to 5.6×10^3 M^{-1} suggest a binding affinity of moderate strength when compared to K_b of classical intercalators such as ethidium ($K_b = 7 \times 10^7$ M^{-1}) [42] or proflavine ($K_b = 4.1 \times 10^5$ M^{-1}) [43], which are 2–4 orders of magnitude higher. But it is only one order of magnitude lower when compared to the oxaliplatin drug ($K_b = 4.12 \times 10^4$ M^{-1}) [44]. These results reinforce the hypothesis that the interaction of both the complexes and their irradiated forms with DNA occurs more as a covalent interaction than as an intercalator.

Cytotoxicity toward A375 cancer cell line. Melanoma is the most serious skin cancer; it comes from the transformation of the melanocytes and has a high probability of spreading and producing metastases with around 20 % mortality [45]. The main cause of melanoma cancer is UV radiation from the sun, together with skin type and genetics [46]. Many treatments have been applied to avoid this dispersion such as surgery, chemotherapy, photodynamic therapy, immunotherapy, radiotherapy, and others, but no treatment has been sufficiently effective [47].

First, the cytotoxicity of ligands (**L1**,**L2**), and the corresponding Pt(II) complexes (**C1**, **C2**) was studied against A375 melanoma cell line. As none of the compounds out of the platforms are soluble in culture media, they had to be diluted in DMF beforehand. Therefore, a previous study was done to determine the % of DMF that A375 cell cultures could tolerate. This resulted in a 0.4 % (*v*/v) DMF as the maximum amount to be used in further assays (Fig. S34). Next, the cytotoxicity of ligands, Pt (II) complexes and their respective photoproducts after irradiation at 365 nm was compared. To this aim, the effect on cell viability of **L1**, **L2**, **C1**, **C2**, and the respective photoproducts (**L1'**, **L2'**, **C1'**, **C2'**) was evaluated in front of the A375 cancer cell line after 24 h of exposure by MTT assay (Fig. 9).

The maximal inhibitory concentration (IC_{50}) values, calculated from the viability assays, (Table 3) show that the complexes are more cytotoxic than their corresponding ligands. **C1** and **C1'** exhibit IC_{50} around 5 μM, while both **L1** and **L1'** have an IC_{50} of approximately 130 μM, about 26 times higher. On the other hand, **L2** and **L2'** which have an IC_{50} around 100 μM that is 20 times higher than for **C2** and **C2'**, which have an IC_{50} of about 5 μM. From these results it can be concluded that the cytotoxicity of the Pt(II) complexes is significantly higher than those related to the ligands.

2.6. Biological assessment of platforms P1 and P2

Once Pt(II) was confirmed as a requirement to achieve cytotoxicity at low concentrations, the study was undertaken to assess cytotoxicity, under the same conditions, of platforms **P1** and **P2**, containing complexes **C1** and **C2**, respectively.

To provide an idea about the internalization of the nanoplatforms in A375 cells, the cytotoxicity in the dark of both systems was evaluated, using different incubation times before washing, 1, 2, and 4 h at 37 °C, and measuring the cell viability after 24 h (Fig. S35). Platform **P1** resulted in a slightly more cytotoxic than **P2.** When considering the highest concentrations assayed (20 μM), the main difference was observed after 2 h of incubation. Also, for the irradiation tests, two concentrations (0.5 and 2.5 μM for **P1** and 1.0 and 5.0 μM for **P2**) were selected, which correspond to IC_{10} and IC_{30} respectively for each platform. These specific concentrations were selected because under these conditions the platforms exhibit poor cytotoxicity in the absence of light and therefore, they can allow the activity under irradiation to be clearly evaluated.

Platforms **P1** and **P2** were next irradiated in the NIR range. Considering that water also absorbs NIR irradiation and can provoke heating of the cell medium with the concomitant induced cell damaging, it was necessary to find the best conditions of power irradiation at 980 nm in which the upconversion process can take place without causing relevant cell death. After extensive research, it was found that the best conditions were doing cycles of 1 min irradiation at 4.5 W/cm^2 intensity power and 2 min break.

Once the conditions were established, assays were carried out. The concentrations corresponding to IC_{10} and IC_{30} (0.5 μM and 5.0 μM of Pt (II) for **P1** and 2.5 μM and 7.5 μM of Pt(II) for **P2**) were used to study the activity of each platform. Samples with the same concentration were placed on different wells, some of which were irradiated while the others were kept in the dark, as a blank with the same concentrations for comparison. Cells were treated with the different concentrations of each platform for 2 h. After this time, the medium was washed to remove the non-internalized platform. Each selected well was irradiated at 980 nm at 4.5 W/cm^2 with cycles of 1 min laser on and 2 min off for 1 h. After 24 h, the cell viability was determined by MTT assay and compared to results obtained in the dark (Fig. 10).

Both platforms show similar increase of the toxicity as raising the concentration of Pt(II). Also, a significant improvement in cytotoxicity after irradiation was observed confirming the viability of the proposed upconversion process to release Pt(II).

The cell viability calculated at the different concentrations assayed (Table 4) shows that in the case of **P1**, the difference in the presence of light or in the dark for each concentration was smaller than for **P2**. If considering the similar toxicity observed for both complexes before and after irradiation, these slight differences can be explained by the different internalization.

To our knowledge, this is the first work presenting the control of the activity of Pt(II) complexes by transforming deeply penetrating NIR light into UV light through UCNPs as nanotransducers not depending on the Pt(IV)/Pt(II) redox pair. When **P1** and **P2** were exposed to 980 nm radiation, they showed increased inhibitor efficiency. The results presented here may constitute a promising step in the future development of UCNP-facilitated redox-independent Pt(II) delivery systems, opening the way to new UV–vis responsive complexes and to others that were discontinued for that very reason.

Table 2
K_b values and the % hypochromic effect obtained for the interaction of *ct*-DNA and with each Pt(II) complex preparation: **C1**, **C1'**, **C2** and **C2'.** K_b was calculated from the ratio of the intercept to the slope, according to the Benesi-Hildebrand equation after the fitting of the UV–vis data from Fig. S33. The hypochromic effect was calculated in reference to the initial intensity at the wavelength indicated in parentheses.

Complex	K_b (M^{-1})	log K_b	% hypochromic effect (λ in nm)
C1	2.4×10^3	3.38	29 % (358 nm)
C1'	1.8×10^3	3.25	14 % (354 nm)
C2	5.6×10^3	3.75	15 % (363 nm)
C2'	4.0×10^3	3.60	52 % (348 nm)

3. Summary and conclusions

In summary, we have developed two novel photoactive Pt(II) complexes and characterized the photoproducts resulted from the continuous radiation with UV light. These platinum complexes have been loaded into the mPEG-ODA coating of UCNPs giving rise to two new nanoplatforms for the study of the NIR radiation induced release of platinum complexes. Upon exposure to a 980 nm NIR laser, UCNPs emit UV-light demonstrating an efficient triggering of Pt(II) complexes release in both spatially and temporally controlled manner. This is the first time that the release of Pt(II) species promoted by UCNPs is described without depending on the Pt(IV)/Pt(II) redox couple. The Pt (II) release in solution in the dark and upon NIR radiation has been tracked in real-time, which is very stimulating to the practical application of Pt-based nanotherapeutics in medical applications. This type of complexes, being part of the nanoplatforms presented here, can be very inspiring in the development of future biomedical applications related to precise and effective drug delivery systems based on the release of Pt(II) with light as an external stimulus. These Pt(II) complexes, before and

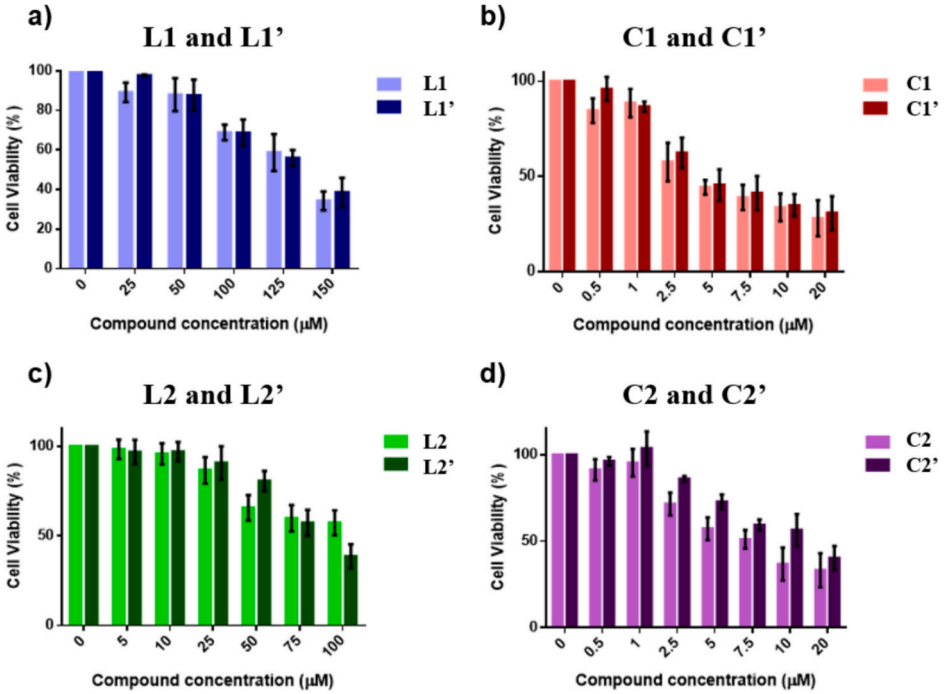

Fig. 9. Effect of a) **L1** and **L1'** b) **C1** and **C1'** c) **L2** and **L2'** d) **C2** and **C2'** on the cell viability of A375 cell line. Cells were exposed to different concentration of each compound for 24 h and cell viability was determined using MTT assays with 3 independent experiments for triplicate.

Table 3
Calculated IC_{50} values for ligands and Pt-complexes before (**L1**, **L2**, **C1**, **C2**) and after (**L1'**, **L2'**, **C1' C2'**) irradiation, and exposure to A375 cells for 24 h.

Ligand	IC_{50} (μM)	Complex	IC_{50} (μM)
L1	130.0 ± 1.0	**C1**	4.7 ± 1.1
L1'	131.0 ± 1.0	**C1'**	5.3 ± 1.1
L2	111.0 ± 1.1	**C2**	4.1 ± 1.1
L2'	84.6 ± 1.5	**C2'**	6.2 ± 1.4

after irradiation, are more cytotoxic than the respective ligands and their photoproducts, leading to the conclusion that Pt(II) plays an important role in preventing cell division.

Platforms **P1** and **P2** were assessed against the A375 cancer cell line. Increasing cytotoxicity for each platform irradiating with NIR light, with a significant difference compared to that in the dark, has been achieved. These results demonstrate an alternative way of activating UV-photoresponsive Pt(II) complexes under NIR radiation through an upconversion process. In addition, the mPEG-ODA coating provides a solution to the common issue concerning low water-solubility of Pt(II) species.

This work reveals how photoactive Pt(II) complexes, with response limited to the UV range, and also very poorly soluble in physiological medium, can be used for NIR-controlled Pt(II) release in physiological medium. We hope that this work will serve as motivation and pave the way for future designs of Pt(II) release systems without being restricted to the need to reduce Pt(IV). We also believe that the approach here presented may stimulate future review of many Pt(II) complexes that were once dismissed because they were not activatable under NIR or were not sufficiently soluble in physiological media.

4. Experimental procedures

Materials. K_2PtCl_4 was purchased from Precious Metal Online. Different organic reagents used for ligands synthesis were purchased from Sigma-Aldrich, Alfa Aesar, Thermo Fisher and Biosynth. Carbon Synth. Organic solvents were dried before use when required. LiAcO (>99 %) and $CaCO_3$(99.5 %) were purchased from Sigma Aldrich. Y_2O_3

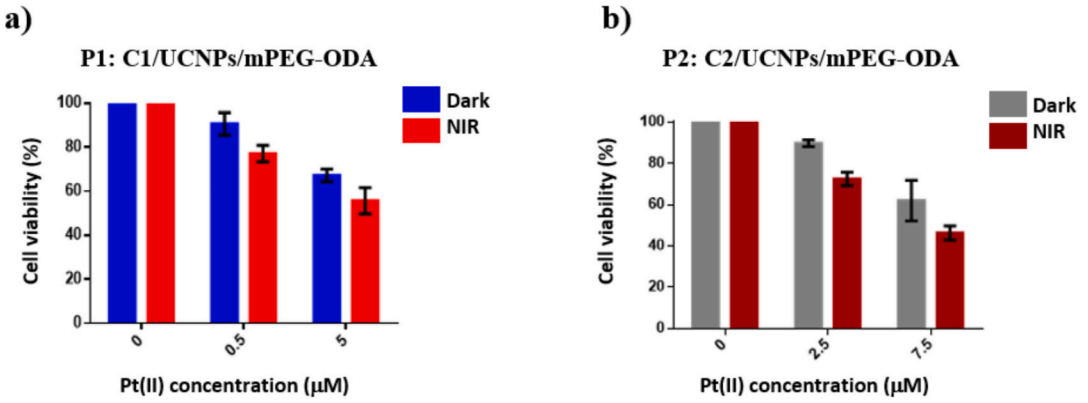

Fig. 10. A375 cell viability *vs.* Pt(II) concentration. All assays consisted in measuring the internalization after 2 h of incubation with a) **C1**/UCNP/mPEG-ODA and b) **C2**/UCNPs/mPEG-ODA.

Table 4
Viability of A375 cells after 2 h of internalization of the platforms and 24 h of incubation after irradiation of NIR light and in the dark.

Entry	Platform	Concentration (μM)	Cell Viability (%)	
			Dark	NIR light
1	**P1**	0.5	91 ± 5.1	77 ± 3.8
2		5.0	67 ± 2.9	56 ± 5.9
3	**P2**	2.5	80 ± 1.6	73 ± 3.3
4		7.5	62 ± 9.8	46 ± 3.2

(99.999 %), Yb_2O_3 (99.999 %), and Tm_2O_3 (99.999 %) were purchased from Sigma Aldrich. Trifluoroacetic acid, hydrochloric acid, ethanol, cyclohexane, dimethyl sulfoxide (DMSO), and dichloromethane (DCM) were purchased from Fischer. Methoxy poly(ethylene glycol) (mPEG, average molecular weight 2000), Octadecylamine (ODA), triethylamine (TEA), Hydroxybenzotriazole (HOBt) and *o*-benzotriazole *N*,*N*,*N*′,*N*′-tetramethyluronium hexafluorophosphate (HBTU) were purchased from Sigma Aldrich. All of the chemical reagents were used as received without further purification.

Characterizations. Fourier transform infrared spectroscopy (FTIR) was performed on a Tensor 27 FT-IR Spectrometer (Bruker) in the range of 400–4000 cm^{-1}. The hydrodynamic size for the nanoparticles were measured by DLS, using the Zetasizer Nano 3600 instrument (Malvern Instruments, UK) equipped with a 633 nm "red" laser. STEM images were performed on a scanning electron microscope Magellan 400 L extreme resolution (XHR) at a voltage of 20 kV. Carbon coated copper grid was used as support. STEM images and EDX scan profiles were also obtained with a FEI Tecnai G2 F20 coupled to an EDAX detector. Observations were performed at room temperature at a voltage of 200 kV. FT-IR spectra were collected. Emission spectra of UCNPs as solid powders were recorded in reflection mode on a custom-made spectrofluorometer where photons emitted are detected using an Andor ICCD camera coupled to a spectrograph. Excitation was conducted with a NIR laser (λ_{exc} = 980 nm, 140 mW) focused on the sample with a NA = 0.25 objective. All of fluorescence studies were performed at room temperature. Ultraviolet−visible (UV − vis) absorption spectroscopy was performed on a HP8453 UV − vis spectrophotometer. ^{1}H NMR spectra were collected by a Bruker spectrometer DPX-360, and 400 MHz instruments and ^{13}C NMR spectra were collected by a Bruker AR430, 101 MHz instrument. Mass spectrometry (MS) and high-resolution mass spectrometry (HRMS) spectra were recorded in a MicroTOF-Q (Brucker Daltonics GmbH, Bremen, Germany) instrument equipped with an electrospray ionization source (ESI) in positive mode. Inductively coupled Plasma-Optical emission Spectroscopy (ICP-OES) was employed to quantify the amount of Pt(II) released from both platforms. The analyses were performed on Agilent 5900 apparatus of samples previously digested in HCl/HNO_3. Ultracentrifugations to obtain HPLC samples were performed in a Oltoalresa Biocen 22R apparatus,15.000 rpm, 5 min at 7 °C. HPLC analyses were collected by an Agilent Technologies 1100 Series apparatus in reversed phase and Waters Xterra©MSC18 3.5 μm, 100 × 2,1 mm column.

4.1. Synthesis

***Synthesis of N,N′-(cyclohexane-1,2-diyl) bis(1-(4,5-dimethoxy-2-nitrophenyl) methanimine)* (3):** (±)-*trans*-1,2-diaminocyclohexane (604 μL, 4.63 mmol) was added to a solution of 3,4-dimethoxy-6-nitrobenzaldehyde (**1**) (2000 mg, 9.44 mmol) and 4 Å molecular sieves in anhydrous THF (20 mL). The mixture was stirred overnight at room temperature under an argon atmosphere. DCM was added, and the resulting mixture was filtered through silica, the filtrate was evaporated under vacuum to give a yellow solid. This crude solid was recrystallized from absolute ethanol to yield diamine **3** as a yellowish solid (1618 mg, 69 %). ^{1}H NMR (400 MHz, $CDCl_3$): δ = 8.72 (s, 2H), 7.49 (s, 2H), 7.42 (s, 2H), 3.96 (s, 6H), 3.93 (s, 6H), 3.61–3.49 (m, 2H), 2.0–0.7 (m, 4H). ^{13}C NMR (100 MHz, $CDCl_3$): δ = 156.9, 153.3, 150.1, 141.8, 126.4, 110.3, 107.1, 74.2, 56.7, 32.9, 24.5 MS (ESI^+): calculated for $[C_{24}H_{28}N_4O_8]$: 501.199 $[M + H]^+$, found: 501.199 $[M + H]^+$.

***Synthesis of N^1,N^2-bis(4,5-dimethoxy-2-nitrobenzyl) cyclohexane-1,2-diamine* (L1):** Diimine **3** (700 mg, 1.39 mmol) and sodium cyanoborohydride (220 mg, 3.49 mmol) with 6.5 mL of glacial acetic acid were stirred at room temperature for 5 min. After 5 min 7 mL of MeOH were added and stirring was continued for 1 h. The solution was evaporated under vacuum. A solution of potassium hydroxide was added up to basic pH and extracted with DCM. The DCM layer was dried over anhydrous Na_2SO_4, filtered, and evaporated to give a yellow solid. The solid was purified with silica gel flash chromatography with DCM:MeOH (9.5:0.5) + 2 % of TEA to give **L1** as a yellow solid (683 mg, 97 %). ^{1}H NMR (400 MHz, $CDCl_3$): δ = 8.72 (s, 2H), 7.49 (s, 2H), 7.42 (s, 2H), 3,96 (s, 6H), 3,93 (s, 6H), 3.55 (m, 2H), 1,98–1.70 (m, 6H), 1,51 (m, 2H). ^{13}C NMR (100 MHz, $CDCl_3$): δ = 153.4, 147.1, 141.1, 131.7, 112.9, 108.2, 61.6, 56.6, 48.6, 31.8, 25.1 MS (ESI^+): calculated for $[C_{24}H_{32}N_4O_8]$: 505.230 $[M + H]^+$, found: 505.230 $[M + H]^+$.

***Synthesis of* C1:** A solution of **L1** (65 mg, 0.130 mmol) in THF (2 mL) was added to an aqueous solution that contained the equivalent amount of K_2PtCl_4 (54 mg, 0.130 mmol). THF was added to the solution until all the solution was dissolved, the reaction was stirred at room temperature overnight. After this time, an orange solid was precipitated which was filtered and washed with acetone to give **C1** as an orange solid (61 mg, 61 %). ^{1}H NMR (400 MHz, DMF-d_7) δ = 8.68 (s, 1H), 7.78 (s, 1H), 7.69 (s, 1H), 7.65 (s, 1H), 6.62 (bs, 2H), 4.91 (bd, J = 16 Hz, 1H), 4.59 (bdd, J = 13.7 Hz, J = 6.2 Hz, 1H), 4.30–3,80 (m, 2H), 4.15 (s, 3H), 4.07 (s, 3H), 4.05 (s, 3H), 3.97 (s, 3H), 3.39 (m, 1H), 3,04 (m, 1H), 1.68–0.68 (m, 8H). ^{13}C NMR (400 MHz, DMF-d_7) δ = 153.2, 153.0, 149.2, 148.8, 143.1, 141.3, 126.3, 124.7, 116.5, 115.7, 108.2, 108.1, 71.2, 63.6, 56.5, 56.4, 56.1, 55.9, 50.3, 49.0, 24.7, 24.5 HRMS (ESI^+): calculated for $[C_{24}H_{32}Cl_2N_4O_8Pt]$: 788.1572 $[M + NH_4]^+$, found: 788.1592 $[M + NH_4]^+$, 813.1686 $[M - Cl^- + dmso]^+$, found 813.1703 $[M - Cl^- + dmso]^+$.

***Synthesis of N,N′-(cyclohexane-1,2-diyl) bis(1-(3,4-dimethoxyphenyl)methanimine)* (9)** [36]: To a solution of benzaldehyde **8** (2000 mg, 12 mmol) in DCM (4 mL) with 4 Å molecular sieves at room temperature, (±)-1,2-diaminocyclohexane (680 mg, 5.96 mmol) was added. The reaction mixture was stirred for 2 h and then filtered. The resulting filtrate was evaporated under vacuum to give a solid that was purified by a recrystallization from absolute ethanol to give **9** as a yellow solid (1861 mg, 76 %) ^{1}H NMR (360 MHz, $CDCl_3$): δ = 8.09 (s, 2H), 7.24 (d, J = 1.3 Hz, 2H), 7.02–6.99 (dd, J = 8.1 Hz, J = 1.3, 2H), 6.78–6.76 (d, J = 8.1 Hz, 2H), 3.87 (s, 6H), 3.86 (s, 6H), 3.36–3.34 (d, 2H), 1.95–1.43 (m, 8H).

***Synthesis of (1SR,2SR)-N^1,N^2-bis((SR)-1-(3,4-dimethoxyphenyl) ethyl)cyclohexane-1,2-diamine* (7):** Methyllithium (1.6 M in Et_2O, 4.10 mmol, 2.56 mL) was added to stirred solution of the diimine **9** in THF (15 mL) which was previously cooled at −78 °C. After 30 min, the reaction mixture was slowly warmed up to 0 °C, stirred for a further 2 h, and then quenched with saturated aq. $NaHCO_3$. The organic phase was extracted with EtOAc and the organic layers were collected, dried over Na_2SO_4 and concentrated to give the crude product. Flash column chromatography (Al_2O_3), eluting with *n*-hexane /EtOAc (1:1), gave a yellow oil that was characterized as a single diastereomer of diamine **7** (403 mg, 90 %). ^{1}H NMR (360 MHz, $CDCl_3$): δ = 6.95 (d, J = 1.8 Hz, 2H), 6.87 (dd, J = 8.2 Hz, J = 1.8 Hz, 2H), 6.80 (d, J = 8.2 Hz, 2H), 3.89 (s, 6H), 3.87 (s, 6H), 3.80 (q, J = 6.5 Hz, 2H), 2.24 (m, 2H), 1.76 (m, 2H), 1.56 (m, 2H), 1.31 (d, J = 6.5 Hz, 6H), 1.10 (m, 2H), 0.89 (m, 2H). ^{13}C NMR (100 MHz, $CDCl_3$): δ = 148.9, 147.8, 140.4, 118.47, 110.9, 109.7, 60.5, 56.0, 56.0, 56.0, 32.8, 25.1, 24.2 HRMS (ESI^+): calculated for $[C_{26}H_{38}N_2O_4]$: 443.2904 $[M + H]^+$, found: 443.2897 $[M + H]^+$.

***Synthesis of (1SR,2SR)-N^1,N^2-bis((SR)-1-(4,5-dimethoxy-2-nitrophenyl)ethyl)cyclohexane-1,2-diamine* (L2):** To a solution of 5.80 mL of HNO_3 60 % in an ice-bath, acetic anhydride (0.984 mL) was added and stirred for 10 min. To that solution, **7** (2.091 g, 4.73 mmol) was

added. The reaction was stirred for another 3 h and then poured into water. A solution of potassium hydroxide was added up to basic pH and the resulting mixture was extracted with DCM. The organic phase was dried over Na_2SO_4 and concentrated under vacuum. Flash column chromatography, eluting with DCM: EtOAc (1:1) + 2 % TEA, gave a yellow solid that was characterized as **L2** (Single diastereomer, 2.287 g, 91 %). ^{1}H NMR (360 MHz, $CDCl_3$): $\delta = 7.45$ (s, 2H), 7.43 (s, 2H), 4.56 (q, $J = 6.3$ Hz, 2H), 4.01 (s, 6H), 3.93 (s, 6H), 2.23 (m, 2H), 1.69 (m, 2H), 1.53 (m, 2H), 1.39 (d, $J = 6.3$ Hz, 6H), 1.06 (m, 2H), 0.85 (m, 2H). ^{13}C NMR (100 MHz, $CDCl_3$): $\delta = 153.0$, 147.3, 140.7, 138.0, 110.2, 107.5, 61.3, 56.3, 51.3, 32.9, 24.8, 23.8 HRMS (ESI^+): calculated for $[C_{26}H_{36}N_4O_8]$: 533.2606 $[M + H]^+$, found: 533.2591 $[M + H]^+$.

***Synthesis of* C2:** A solution of **L2** (50 mg, 0.094 mmol) in THF (2 mL) was added to a water solution of an equivalent amount of K_2PtCl_4. THF was added to the mixture up to complete dissolution. After stirring overnight at room temperature, a brown solid was obtained which was filtered. The solid was purified by precipitation in acetone/Et_2O and identified as **C2** (21 mg, 28 %). ^{1}H NMR (400 MHz, $CDCl_3$) $\delta = 7.48$ (s, 1H), 7.33 (s, 1H), 7.26 (s, 1H), 7.01 (s, 1H), 5,56 (bs, 1H), 5,33 (bs, 1H), 5,11 (bs, 1H), 4,40 (bs, 1H), 4.35 (s, 3H), 4,01 (s, 6H), 3,90 (s, 3H), 3,31 (bs, 1H), 2,60 (bs, 1H), 2,00 (bd, 2H), 1.76 (d, $J = 4$ Hz, 3H), 1.40 (d, $J = 8$ Hz, 3H), 2.00–0,50 (m, 6H). ^{13}C NMR (100 MHz, $CDCl_3$): $\delta = 153.6$, 152.9, 149.0, 148.5, 141.9, 140.5, 131.0, 130.7, 115.5, 110.9, 107.7, 107.0, 72.1, 71.9, 64.0, 57.7, 56.9, 56.6, 56.4, 48.9, 31.6, 30.0, 26.2, 25.3, 25.1, 23.5 HRMS (ESI^+): calculated for $[C_{26}H_{36}Cl_2N_4O_8Pt]$: 821.1439 $[M + Na]^+$, found: 821.1461 $[M + Na]^+$.

***Synthesis of LiYF$_4$; Yb^{3+}; Tm^{3+} nanoparticles*:** $LiYF_4$; Yb^{3+}; Tm^{3+} UCNPs were synthesized *via* thermal decomposition, as a two-step process. In the first step, a mixture of water/trifluoroacetic acid (1:1) (10 mL), was added to a 2-neck round-bottom flask containing Tm_2O_3 (0.0024 g, 6.25×10^{-3} mmol, 0.5 mol% Tm^{3+}), Yb_2O_3 (0.1232 g, 3.13×10^{-1} mmol, 2.5 mol% Yb^{3+}) and Y_2O_3 (0.2103 g, 9.31×10^{-1} mmol). The cloudy solution was heated at 80 °C until it was clear. The resulting solution was heated at 60 °C for 5 h to form the Y^{+3}, Yb^{3+}, and Tm^{3+} trifluoroacetate precursors, then the solvent was evaporated under pressure. In the second step, $LiAcO{\cdot}2H_2O$ (160 mg, 1.6 mmol) was added to the dried precursor mixture (655 mg), with oleic acid (10 mL) and 1-octadecene (10 mL) and the final mixture was degassed for 30 min at 120 °C. The temperature was increased at a rate of 15 °C/min to 330 °C. Then, the reaction mixture was stirred at 330 °C for 1 h. After cooling to room temperature absolute ethanol was added to precipitate $LiYF_4$, Yb^{3+}, and Tm^{3+} UCNPs, which were subsequently isolated *via* centrifugation (3000 rpm, 15 min). The pellet was washed with a 1:3 hexane/ethanol mixture twice to remove any impurities.

***Synthesis of P1: C1/UCNPs/mPEG-ODA*:** 110 mg of mPEG-ODA, 10 mg of **C1** and 20 mg of UCNPs were mixed in 2 mL of $CHCl_3$. The mixture was sonicated for 5 min and THF (1 mL) was added to the mixture. After 5 min under sonification, 6 mL of water were added to the mixture and sonicated for 3 h to evaporate $CHCl_3$ and THF, keeping the water bath of the sonicator below 50 °C. Then, the resulting solution was added to a falcon tube and centrifuged at 4000 rpm for 2 h, excess mPEG-ODA in supernatant was removed. The resulting nanoparticles were dispersed in water and filtered through a 0.45 μm syringe filter to remove large aggregates and possible mPEG-ODA traces. After that, the solvent was removed by lyophilization overnight.

Synthesis of P2: C2/UCNPs/mPEG-ODA: 110 mg of mPEG-ODA, 11 mg of **C2** and 20 mg of UCNPs were mixed in 2 mL of $CHCl_3$. Then the mixture was sonicated for 5 min. After this time, 6 mL of water was added to the mixture and sonicated for 3 h to evaporate $CHCl_3$, keeping the water bath of the sonicator below 50 °C. Then, the solution was added to a falcon tube and centrifuged at 4000 rpm for 2 h, excess mPEG-ODA in supernatant was removed. The nanoparticles were dispersed in water and filtered through a 0.45 μm syringe filter to remove large aggregates. After that, the solvent was removed by lyophilization overnight.

4.2. Pt (II)-release experiment

ICP-OES: As a general procedure, the corresponding amounts of **P1** or **P2** to 80 μg Pt(II) were suspended in 2 mL of PBS solution. This suspension was introduced in a polypropylene cuvette with 1 mm holes (*ca.* 9 per cm^2) tightly surrounded by a dialysis bag (3 nm pore). The cuvette was placed in 65 mL of a PBS surrounding bath at 37 °C. The cuvette was then irradiated under UV-light (365 nm) or NIR light (980 nm) or kept in the dark. Aliquots (1 mL) were collected from the PBS surrounding bath at different times and replaced with the same volume of fresh PBS (See table S1). The aliquots were digested with HCl 1 % (*v*/v) and HNO_3 1 % (v/v) and analyzed by ICP-OES.

HPLC: Equal platform **P2** samples were suspended in milliQ water (2 mg/200 μL) were subjected to UV (365 nm, W·cm-2) and NIR (980 nm, W·cm-2) irradiation while another sample was left in the dark. While irradiation, samples were ventilated to avoid temperature increase due to the radiation itself. After 3 h under irradiation or darkness, all three samples were subjected to ultracentrifugation and samples of the supernatant were taken. These samples were analyzed by HPLC. Method: H_2O:ACN from 80:20 to 5:95, 10 min, 5:95, 5 min, from 5:95 to 80:20 in 1 min, 80:20, 9 min, const. Flow: 0.3 mL min^{-1}.

4.3. Cell viability assays

Cell culture: A375 human melanoma cell line was acquired from the European Collection of Authenticated Cell Cultures (ECACC). Cells were cultured at 37 °C under 5 % CO_2 in DMEM culture medium, supplemented with 10 % FBS, 2 mM L-glutamine, 1 % penicillin–streptomycin (100 U/mL penicillin, 100 μg/mL streptomycin) and 1 % fungizone (250 U/mL). Cells were monitored to ensure satisfactory confluence and morphology using an inverted phase-contrast Eclipse TS100 microscope (Nikon, Tokyo, Japan). When 70–80 % of confluence was reached, cells were treated with trypsin-EDTA (0.25 % trypsin and 1 mM EDTA) and used in the *in vitro* cell viability assays.

Cytotoxicity of ligands and complexes: Stock solutions were freshly prepared in DMF for **L1**, **L2**, **C1**, **C2**. To prepare **L1'**, **L2'**, **C1'**, and **C2'** stocks, half of volume of stock of each compound (**L1**, **L2**, **C1**, **C2**) was taken and irradiated with UV lamp at 365 nm for 2 h. Each stock solutions were diluted in the culture medium for working concentrations (maximum 0.2 % DMF in biological experiments). Stock solutions were freshly prepared in water for **C1**/UCNPs/mPEG-ODA (**P1**) and **C2**/UCNPs/mPEG-ODA (**P2**). Each stock solution was diluted in the culture medium for working concentrations.

A375 cells were seeded in 96-well plates at 40000 cells/mL for 24 h of exposure. After 24 h, medium was replaced with fresh medium containing: (i) **L1** and **L1'** (0, 25, 50, 100, 125, 150 μM), (ii) **L2** and **L2'** (0, 5, 10, 25, 50, 75, 100 μM), (iii) **C1** and **C1'** (0, 0.5, 1, 2.5, 5, 7.5, 10, 20 μM), (iv) **C2** and **C2'** (0, 0.5, 1, 2.5, 5, 7.5, 10, 20 μM) and incubated for 24 h. At the end of the incubation time, the medium was removed from each well and replaced by fresh culture medium with 50 μL of MTT (1 mg/mL in PBS) and incubated for 4 h at 37 °C in a 5 % CO_2 humified atmosphere. Thereafter, the culture medium with MTT was removed and replaced by 150 μL of DMSO to dissolve the formazan crystals. The absorbance was measured with a plate reader (Synergy HT Multi-Mode, BioTek, Winoski, VT) at 570 nm with blank corrections.

Cytotoxicity of NIR activated nanoplatforms: For the study of the *in vitro* cytotoxicity of **P1** and **P2**, A375 cells were seeded in 96-well plates as described above. After 24 h, medium was replaced with fresh medium containing **P1** (0, 0.5, 5 μM of Pt(II)) or **P2** (0, 2.5, 7.5 μM of Pt(II)) and incubated for 2 h. After the incubation time, the supernatant was removed to discard what was not internalized and new medium was added. Subsequently, wells were irradiated at 980 nm with a power intensity of 4.5 W/cm^2 for 60 min (repeating the sequence: 1 min of irradiation after 2 min break to avoid photothermal effects). Then the cells were incubated for another 24 h. Cell viability was evaluated as described above.

CRediT authorship contribution statement

Marc-Ricard Batten: Investigation. **Josep Antoni Gutiérrez-Orgaz:** Investigation. **Fernando Eduardo Maturi:** Writing – review & editing, Investigation. **Luís Dias Carlos:** Investigation. **Helena Oliveira:** Writing – review & editing, Investigation. **Jordi Hernando:** Writing – review & editing, Investigation. **Fernando Novio:** Writing – review & editing, Methodology, Investigation. **Antonio Rodríguez-Diéguez:** Investigation. **Mercè Capdevila:** Writing – review & editing. **Òscar Palacios:** Writing – review & editing, Conceptualization. **Pau Bayón:** Writing – review & editing, Writing – original draft, Investigation, Formal analysis, Data curation, Conceptualization.

Funding

Financial support was provided by the Spanish *Ministerio de Ciencia e Innovación* through the project: PID2022-138479NB-I00. M. C., Ò. P., and P. B. are members of the "*Grups de Recerca"- Generalitat de Catalunya*, ref. 2021SGR00668. J. H. thanks *Agència de Gestió d'Ajuts Universitaris i de Recerca* (AGAUR)-*Generalitat de Catalunya* for its support through the project ref. 2021SGR00064. F. N. thanks MICIU/AEI/10.13039/501100011033 and European Union Next Generation EU/PRTR for their support with grant CNS2022–136106. F. N. also thanks MCIU/AEI/10.13039/501100011033/ and ERDF for grant PID2021–127983OB-C21. F. E. M., L. D. C., and H. O. thank the project CICECO-Aveiro Institute of Materials (UIDB/50011/2020, UIDP/50011/2020 and LA/P/0006/2020) and CESAM (UIDP/50017/2020 and UIDB/50017/2020 and LA/P/0094/2020), financed by national funds through the FCT/MCTES (PIDDAC). This work was also supported by the project PTDC/BTM-MAT/31794/2017 (POCI-01-0145-FEDER-031794), funded by FEDER, through COMPETE2020—*Programa Operacional Competitividade e Internacionalização* (POCI)—and by national funds (OE), through FCT/MCTES.

Declaration of competing interest

The authors declare the following financial interests/personal relationships which may be considered as potential competing interests:

Pau Bayon reports financial support was provided by Spain Ministry of Science and Innovation. Oscar Palacios, Merce Capdevila reports financial support was provided by Spain Ministry of Science and Innovation. Pau Bayon reports administrative support was provided by Government of Catalonia. Oscar Palacios, Merce Capdevila reports administrative support was provided by Government of Catalonia. Jordi Hernando reports financial support was provided by Government of Catalonia Agency for Administration of University and Research Grants. Fernando Novio reports financial support was provided by Spain Ministry of Science, Innovation and Universities. Fernando Novio reports financial support was provided by European Union. Helena Oliveira, Fernando Eduardo Maturi, Luis Carlos Dias reports financial support was provided by Foundation for Science and Technology. Helena Oliveira, Fernando Eduardo Maturi, Luis Carlos Dias reports financial support was provided by Compete 2020-POCI. If there are other authors, they declare that they have no known competing financial interests or personal relationships that could have appeared to influence the work reported in this paper.

Acknowledgments

Authors acknowledge the SynOrgFun Group at UAB, Chemistry Department, for its valuable support.

Appendix A. Supplementary data

Supplementary data to this article can be found online at https://doi.org/10.1016/j.jinorgbio.2025.112982.

Data availability

The data supporting this article have been included as part of the Supplementary Information. Crystallographic data for the structures reported in this manuscript have been deposited with the Cambridge Crystallographic Data Centre under the CCDC numbers: 2320458 (Compound **L2**), and 232459 (Compound **11**). Copies of these data can be obtained free of charge from http://www.ccdc.cam.ac.uk/data_request/cif.

References

[1] a) L. Kathryn, K.L. Haas, K.J. Franz, Application of metal coordination chemistry to explore and manipulate cell biology, Chem. Rev. 109 (2009) 4921–4960; b) K.D. Mjos, C. Orvig, Metallodrugs in medicinal inorganic chemistry, Chem. Rev. 114 (2014) 4540–4563.

[2] E. Boros, P.J. Dyson, G. Gasser, Classification of metal-based drugs according to their mechanisms of action, Chem 6 (2020) 41–60.

[3] a) E. Ortega-Forte, A. Rovira, M. López-Corrales, A. Hernández-García, F. J. Ballester, E. Izquierdo-García, M. Jordà-Redondo, M. Bosch, S. Nonell, M. D. Santana, J. Ruiz, V. Marchán, G. Gasser, A near-infrared light-activatable Ru(II)-coumarin photosensitizer active under hypoxic conditions, Chem. Sci. 14 (2023) 7170–7184 (and references therein); b) L. Gourdon, K. Cariou, G. Gasser, Phototherapeutic anticancer strategies with first-row transition metal complexes: a critical review, Chem. Soc. Rev. 51 (2022) 1167–1195; c) F. Lermyte, R.J. Needham, M. Palau, P.J. Sadler, H. Shi, F.-X. Wang, W.-Y. Zhang, Z. Zhang, Metallodrugs are unique: opportunities and challenges of discovery and development, Chem. Sci. 11 (2020) 12888–12917 (and references therein); d) N.J. Farrer, L. Salassa, P.J. Sadler, Photoactivated chemotherapy (PACT): the potential of excited-state d-block metals in medicine, Dalton Trans. (2009) 10690–10701.

[4] K.L. Ciesienski, L.M. Hyman, D.T. Yang, K.L. Haas, M.G. Dickens, R.J. Holbrook, K. J. Franz, A photo-caged platinum(II) complex that increases cytotoxicity upon light activation, Eur. J. Inorg. Chem. (2010) 2224–2228.

[5] S. Bonnet, Why develop photoactivated chemotherapy? Dalton Trans. 47 (2018) 10330–10343.

[6] S. Bonnet, Shifting the light activation of metallodrugs to the red and near-infrared region in anticancer phototherapy, Comment. Inorg. Chem. 35 (2015) 179–213 (and references therein).

[7] For some recent examples of the use of irradiation-responsive complexes in NIR: a) Wahengbam, S.; Musib, D.; Roy, M. Recent advances on the development of early transition metal complexes for photo-assisted cytotoxicity applications. *ChemistrySelect.* 2024, 9, e202302969– e202302991. b) W. Jiang, L. Lin, P. Wu, H. Lin, J. Su, Near-infrared-II nanomaterials for activatable photodiagnosis and phototherapy, Chem. Eur. J. 30 (2024) e202400816.

[8] C. Ash, M. Dubec, K. Donnel, T. Bashford, Effect of wavelength and beam width on penetration in light-tissue interaction using computational methods, Lasers Med. Sci. 32 (2017) 1909–1918.

[9] R. Kadokawa, T. Fujie, G. Sharma, K. Ishibashi, K. Ninomiya, K. Takahashi, E. Hirata, K. Kuroda, High loading of trimethylglycine promotes aqueous solubility of poorly water-soluble cisplatin, Sci. Rep. 11 (2021) 9770–9776.

[10] a) R.J. Browning, P.J.T. Reardon, M. Parhizkar, R.B. Pedley, M. Edirisinghe, J. C. Knowles, E. Stride, Drug delivery strategies for platinum-based chemotherapy, ACS Nano 11 (2017) 8560–8578; b) C. Xian, H. Chen, F. Xiong, Y. Fang, H. Huang, J. Wu, Platinum-based chemotherapy via nanocarriers and co-delivery of multiple drugs, Biomater. Sci. 9 (2021) 6023–6036; c) J.-J. Zhang, Q.-J. Xu, Y. Zhang, Q. Zhou, R. Lv, Z. Chen, W. He, Recent advances in nanocarriers for clinical platinum(II) anticancer drugs, Coord. Chem. Rev. 505 (2024) 215676; d) D. Wei, Y. Huang, B. Wang, L. Ma, J. Karges, H. Xiao, Photo-reduction with NIR light of nucleus-targeting PtIV nanoparticles for combined tumor-targeted chemotherapy and photodynamic immunotherapy, Angew. Chem. Int. Ed. 61 (2022) e202201486; e) Y. Wang, Y. Cong, M. Cai, X. Liang, L. Wang, D. Zhou, Charge-conversional click polyprodrug nanomedicine for targeted and synergistic cancer therapy, J. Control. Release 356 (2023) 567–579.

[11] a) P. Ma, H. Xiao, C. Li, Y. Dai, Z. Cheng, Z. Hou, J. Lin, Inorganic nanocarriers for platinum drug delivery, Mater. Today 18 (2015) 554–564; b) T.C. Johnstone, K. Suntharalingam, S.J. Lippard, The next generation of platinum drugs: targeted Pt(II) agents, nanoparticle delivery, and Pt(IV) prodrugs, Chem. Rev. 116 (2016) 3436–3486; c) C. Xiao, H. Hu, H. Yang, S. Li, H. Zhou, J. Ruan, Y. Zhu, X. Yangabd, Z. Li, Colloidal hydroxyethyl starch for tumor-targeted platinum delivery, Nanoscale Adv. 1 (2019) 1002–1012; d) A. Quarta, M. Amorín, M.J. Aldegunde, L. Blasi, A. Ragusa, S. Nitti, G. Pugliese, G. Gigli, J.R. Granja, T. Pellegrino, Novel synthesis of platinum complexes and their intracellular delivery to tumor cells by means of magnetic nanoparticles, Nanoscale 11 (2019) 23482–23497; e) K. Matha, G. Lolloc, G. Taurinod, R. Respaude, I. Marigog, M. Shariatih,

O. Bussolatid, A. Vermeuleni, K. Remauth, J.-P. Benoita, Bioinspired hyaluronic acid and polyarginine nanoparticles for DACH Pt delivery, Eur. J. Pharm. Biopharm. 150 (2020) 1–13;
f) P. Xie, Y. Wang, D. Wei, L. Zhang, B. Zhang, H. Xiao, H. Song, X. Mao, Nanoparticle-based drug delivery systems with platinum drugs for overcoming cancer drug resistance, J. Mater. Chem. B 9 (2021) 5173–5194;
g) X. Zhao, G. Zhang, J. Ke, J. Wang, H. Zhuo, Enhanced in vitro cytotoxicity and in vivo nursing care of gastric cancer cells by nanoparticles bearing platinum (IV) prodrug of cisplatin, J. Biomed. Nanotechnol. 19 (2023) 416–423;
h) W. Wanga, X. Hea, X. Wanga, T. Zhaoa, O. Muraoka, G. Tanabe, W. Xiec, T. Zhoua, L. Xinga, Q. Jind, H. Jiang, Glutathione-depleted cyclodextrin pseudo-polyrotaxane nanoparticles for anti-inflammatory oxaliplatin (IV) prodrug delivery and enhanced colorectal cancer therapy, Chin. Chem. Lett. 35 (2024) 108656.

[12] C. Zhang, C. Xu, X. Gao, Q. Yao, Platinum-based drugs for cancer therapy and anti-tumor strategies, Theranostics *12* (**2022**) 2115–2132.

[13] R.S. Ajee, P.S. Roy, S. Dey, S. Sundaresan, Upconversion nanoparticles and their potential in the realm of biomedical sciences and theranostics, J. Nanopart. Res. 26 (2024) 50.

[14] A. Sedlmeier, H.H. Gorris, Surface modification and characterization of photon-upconverting nanoparticles for bioanalytical applications, Chem. Soc. Rev. 44 (2015) 1526–1560.

[15] E. Hemmer, A. Benayas, F. Légaré, F. Vetrone, Exploiting the biological windows: current perspectives on fluorescent bioprobes emitting above 1000 nm, Nanoscale Horiz. 1 (2016) 168–184.

[16] a) E. Wexselblatt, D. Gibson, What do we know about the reduction of Pt(IV) pro-drugs? J. Inorg. Biochem. 117 (2012) 220–229;
b) Y. Dai, X. Kang, D. Yang, X. Li, X. Zhang, C. Li, Z. Hou, Z. Cheng, P. Ma, J. Lin, Platinum (IV) pro-drug conjugated $NaYF_4$:Yb^{3+}/Er^{3+} nanoparticles for targeted drug delivery and up-conversion cell imaging, Adv. Healthc. Mater. 2 (2013) 562–567;
c) Y. Dai, H. Xiao, J. Liu, Q. Yuan, P. Ma, D. Yang, C. Li, Z. Cheng, Z. Hou, P. Yang, J. Lin, In vivo multimodality imaging and cancer therapy by near-infrared light triggered trans-platinum pro-drug-conjugated upconversion nanoparticles, J. Am. Chem. Soc. 135 (2013) 18920–18929;
d) Y. Min, J. Li, F. Liu, E.K.L. Yeow, B. Xing, Near-infrared light-mediated photoactivation of a platinum antitumor prodrug and simultaneous cellular apoptosis imaging by upconversion-luminescent nanoparticles, Angew. Chem. Int. Ed. 53 (2014) 1012–1016;
e) E. Ruggiero, J. Hernandez-Gil, J.C. Mareque-Rivas, L. Salassa, Near infrared activation of an anticancer Pt complex by Tm-doped upconversion nanoparticles, Chem. Commun. 51 (2015) 2091–2094;
f) F. Ai, T. Sun, Z. Xu, Z. Wang, W. Kong, M.W. To, F. Wang, G. Zhu, An upconversion nanoplatform for simultaneous photodynamic therapy and Pt chemotherapy to combat cisplatin resistance, Dalton Trans. 45 (2016) 13052–13060;
g) S. Perfahl, M.M. Natile, H.S. Mohamad, C.A. Helm, C. Schulzke, G. Natile, P. J. Bednarski, Mol. Pharm. 13 (2016) 2346–2362;
h) B. Teng, P. Ma, C. Yu, X. Zhang, Q. Feng, L. Wen, C. Li, Z. Cheng, D. Jind, J. Lin, Upconversion nanoparticles loaded with eIF4E siRNA and platinum(IV) prodrug to sensitize platinum-based chemotherapy for laryngeal cancer and bioimaging, J. Mater. Chem. B 5 (2016) 307–317;
i) Y. Dai, H. Bi, X. Deng, C. Li, F. He, P. Ma, P. Yang, J. Lin, 808 nm near-infrared light controlled dual-drug release and cancer therapy in vivo by upconversion mesoporous silica nanostructures, J. Mater. Chem. B Mater. Biol. Med. 5 (2017) 2086–2095;
j) S. Xu, X. Zhu, C. Zhang, W. Huang, Y. Zhou, D. Yan, Oxygen and Pt(II) self-generating conjugate for synergistic photo-chemo therapy of hypoxic tumor, Nat. Commun. 9 (2018) 1–9;
k) H. Bi, Y. Dai, P. Yang, J. Xu, D. Yang, S. Gai, F. He, B. Liu, C. Zhong, A. An, J. Lin, Glutathione mediated size-tunable UCNPs-Pt(IV)-$ZnFe_2O_4$ nanocomposite for multiple bioimaging guided synergetic therapy, Small 14 (2018) 1703809–1703822;
l) B. Teng, Y. Han, X. Zhang, H. Xiao, C. Yu, H. Li, Z. Cheng, D. Jin, K.-L. Wong, P. Ma, J. Lin, Phenanthriplatin(IV) conjugated multifunctional up-converting nanoparticles for drug delivery and biomedical imaging, J. Mater. Chem. B 6 (2018) 5059–5068;
m) S. Xu, X. Zhu, C. Zhang, W. Huang, Y. Zhou, D. Yan, Oxygen and Pt(II) self-generating conjugate for synergistic photo-chemo therapy of hypoxic tumor, Nat. Commun. 9 (2018) 2053;
n) Q. Zhang, G. Kuang, S. He, H. Lu, Y. Cheng, D. Zhou, Y. Huang, Photoactivatable prodrug-backboned polymeric nanoparticles for efficient light-controlled gene delivery and synergistic treatment of platinum-resistant ovarian cancer, Nano Lett. 20 (2020) 3039–3049;
o) B. Teng, B. Ding, S. Shao, Z. Wang, W. Tong, S. Wang, Z. Cheng, J. Lin, P. Ma, Intracellular RNA and nuclear DNA-dual-targeted tumor therapy via upconversion nanoplatforms with UCL/MR dual-mode bioimaging, Chem. Eng. J. 405 (2021) 126606;
p) G. Kuang, H. Lu, S. He, H. Xiong, J. Yu, Q. Zhang, Y. Huang, Near-infrared light-triggered polyprodrug/siRNA loaded upconversion nanoparticles for multi-modality imaging and synergistic cancer therapy, Adv. Healthc. Mater. 10 (2021) 2100938–2100949;
q) P. Jethva, M. Momin, T. Khan, A. Omri, Lanthanide-doped upconversion luminescent nanoparticles evolving role in bioimaging, biosensing, and drug delivery, Materials 15 (2022) 2374–2396;
r) Y. Chen, Y. Yang, S. Du, J. Ren, H. Jiang, L. Zhang, J. Zhu, Mitochondria-targeting upconversion nanoparticles@mof for multiple-enhanced photodynamic therapy in hypoxic tumor, ACS Appl. Mater. Interfaces 15 (2023) 35884–35894;
s) Z. Liu, Z. Feng, M. Chen, J. Zhan, R. Wu, Y. Shi, Y. Xue, R. Liu, J.-J. Zhu, J. Zhang, An orthogonally activatable CRISPR-Cas13d nanoprodrug to reverse chemoresistance for enhanced chemo-photodynamic therapy, Chem. Sci. 14 (2023) 4102–4113;
t) X. Yan, Y. Xin, Y. Yu, X. Li, B. Li, M. Elsabahy, J. Zhang, F. Ma, H. Gao, Remotely controllable supramolecular nanomedicine for drug-resistant colorectal cancer therapy caused by fusobacterium nucleatum, Small Meth. 8 (2024) 2301309–2301317;
u) X.-M. Liu, Z.-Z. Zhu, X.-R. He, Y.-H. Zou, Q. Chen, X.-Y. Wang, H.-M. Liu, X. Qiao, X. Wang, J.-Y. Xu, NIR light and GSH dual-responsive upconversion nanoparticles loaded with multifunctional platinum(IV) prodrug and RGD peptide for precise cancer therapy, ACS Appl. Mater. Interfaces 16 (2024) 40753–40766;
v) Y. Wang, L. Wang, T. Li, M. Ouyang, H. Xiong, D. Zhou, Bimetallic nanoparticles as cascade sensitizing amplifiers for low-dose and robust cancer radioimmunotherapy, Acta Pharm. Sin. B 14 (2024) 1787e1800.

[17] M.-R. Batten, NIR Light Controlled Release of Pt(II) by Means of Upconversion Nanoparticles, PhD Thesis,, Universitat Autònoma de Barcelona, 2024, http://hdl.handle.net/10803/691663.

[18] M. Dalai, M. Periasamy, Diastereoselective reductive *N*-alkylation of (*R,R*)-*trans*-1,2-diaminocyclohexane with prochiral ketones using the $Ti(O^iPr)_4/NaBH_4$ system, Tetrahedron Asymmetry 20 (2009) 1247–1253.

[19] M.A. Collins, F.J. Kernozek, Catecholamine-related isoquinoline alkaloids. 1. Synthesis of 4-hydroxytetrahydroisoquinoline analogs of adrenaline and metanephrine, J. Heterocyclic Chem. 9 (1972) 1437–1440.

[20] D. Savoia, A. Gualandi, M. Bandini, Diastereoselective addition of organometallic reagents to diimines derived from (*R,R*)-1,2-diaminocyclohexane and aromatic aldehydes, Lett. Org. Chem. 6 (2009) 434–438.

[21] a) F. Zhang, S. Zhang, X. Duan, Substitution of the nitro group with grignard reagents: facile arylation and alkenylation of pyridine *N*-oxides, Org. Lett. 14 (2012) 5618–5620;
b) K. Liu, F. Zhang, X. Duan, 1,2-addition of alkyl Grignard reagents to the nitro group: simple access to 2-[alkyl(hydroxy)amino]pyridine *N*-oxides and 2-alkylaminopyridine *N*-oxides, Eur. J. Org. Chem. 27 (2013) 6152–6157.

[22] J. Bravo, C. Cativiela, R. Navarro, E.P. Urriolabeitia, Synthesis, characterization and catalytic activity in heck-type reactions of orthometallated PdII and PtII complexes derived from (1*R*,2*R*)-1,2-diaminocyclohexane, J. Organomet. Chem. 650 (2002) 157–172.

[23] M.S. Meijer, P.A. Rojas-Gutierrez, D. Busko, I.A. Howard, F. Frenzel, C. Würth, U. Resch-Genger, B.S. Richards, A. Turshatov, J.A. Capobianco, S. Bonnet, Absolute upconversion quantum yields of blue-emitting $LiYF_4$:Yb^{3+}, Tm^{3+} upconverting nanoparticles, Phys. Chem. Chem. Phys. 20 (2018) 22556–22562.

[24] A.-R. Hong, J.-H. Kyhm, G. Kang, H.S. Jang, Orthogonal R/G/B Upconversion luminescence-based full-color tunable upconversion nanophosphors for transparent displays, Nano Lett. 21 (11) (2021) 4838–4844.

[25] J.T. Mulder, K. Jenkinson, S. Toso, M. Prato, W.H. Evers, S. Bals, L. Manna, A. J. Houtepen, Nucleation and growth of bipyramidal Yb:$LiYF_4$ nanocrystals-growing up in a hot environment, Chem. Mater. 35 (2023) 5311–5321.

[26] W. Chen, M. Chen, Q. Zang, L. Wang, F. Tang, Y. Han, C. Yang, L. Deng, Y.N. Liu, NIR light controlled release of caged hydrogen sulfide based on upconversion nanoparticles, Chem. Commun. 51 (2015) 9193–9196.

[27] a) M. Secu, Upconversion avalanche in the Yb^{3+}/Ho^{3+} doped SiO_2-$LiYF_4$ nano-glass ceramic, Dig. J. Nanomater. Biostruct. 12 (2017) 1075–1080;
b) C. Secu, C. Bartha, C. Radu, M. Secu, Up-conversion luminescence and magnetic properties of multifunctional Er^{3+}/Yb^{3+}-doped SiO_2-GdF_3/ligdF_4 glass ceramics, Magnetochemistry 9 (2023) 11.

[28] V. Mahalingam, F. Vetrone, R. Naccache, A. Speghini, J.A. Capobianco, Colloidal tm^{+3}/Yb^{+3}-doped $LiYF_4$ nanocrystals: multiple luminescence spanning the UV to NIR regions via low-energy excitation, Adv. Mater. 21 (2009) 4025–4028.

[29] B. Malisova, S. Tosatti, M. Textor, K. Gademann, S. Zürcher, Poly(ethylene glycol) Adlayers immobilized to metal oxide substrates through catechol derivatives: influence of assembly conditions on formation and stability, Langmuir 26 (2010) 4018–4026.

[30] At this point, 0.8 μm pore size filter was also tested but nanoparticle aggregates passed through the membrane.

[31] These values were calculated as an average of different batches in the preparation of **P1** and **P2**.

[32] K. Debnath, K. Mandal, N.R. Jana, Phase transfer and surface functionalization of hydrophobic nanoparticle using amphiphilic poly(amino acid), Langmuir 32 (2016) 2798–2807.

[33] P. Klán, T. Šolomek, C.G. Bochet, A. Blanc, R. Givens, M. Rubina, V. Popik, A. Kostikov, J. Wirz, Photoremovable protecting groups in chemistry and biology: reaction mechanisms and efficacy, Chem. Rev. 113 (2013) 119–191.

[34] M. Villabona, S. Wiedbrauk, F. Feist, G. Guirado, J. Hernando, C. Barner-Kowollik, Dual-wavelength gated oxo-diels-alder photoligation, Org. Lett. 23 (2021) 2405–2410.

[35] B. Avila, M.-H. El-Dakdouki, M. Nazer, J.G. Harrison, D.J. Tantillo, M.J. Haddadin, M.J. Kurth, Acid and base catalyzed Davis–Beirut reaction: experimental and theoretical mechanistic studies and synthesis of novel 3-amino-2*H*-indazoles, Tetrahedron Lett. 53 (2012) 6475–6478.

[36] These concentrations were calculated on the basis of the mentioned Pt(II) loading values for platforms **P1** (1%) and **P2** (1.8%) (for more details, see experimental part).

[37] V.I. Ivanov, L.E. Minchenkova, A.K. Schyolkina, A.I. Poletayev, Different conformations of double-stranded nucleic acid in solution as revealed by circular dichroism, Biopolymers 12 (1973) 89–110.

[38] a Y. Figueroa-DePaz, K. Resendiz-Acevedo, S.G. Dávila-Manzanilla, J.C. García-Ramos, L. Ortiz-Frade, J. Serment-Guerrero, L.D.N.A. Ruiz-Azuara, a target of mixed chelate-copper (II) compounds (Casiopeina®) studied by electrophoresis, UV-vis circular dichroism techniques, J. Inorg. Biochem. *231* (2022) 111772;
b) S. Veeralakshmi, S. Nehru, G. Sabapathi, S. Arunachalam, P. Venuvanalingam, P. Kumar, C. Anusha, V. Ravikumar, Single and double chain surfactant-cobalt(III) complexes: the impact of hydrophobic on the interactions with calf thymus DNA, and their biological activities, RSC Adv. 5 (2015) 31746–31758;
c) A.M. Polyanichko, V.V. Andrushchenko, E.V. Chikhirzhina, V.I. Vorob'ev, H. Wieser, The effect of managanese(II) on DNA structure: electronic and vibrational circular dichroism studies, Nucleic Acids Res. 32 (2004) 989–996;
d) K. Naing, M. Takahashi, M. Taniguchi, A. Yamagishi, Interactions of enantiomeric ruthenium(II) complexes with polynucleotides as studied by circular dichroism, electric dichroism measurements, and photolysis, Inorg. Chem. 34 (1995) 350–356;
e) A.M. Tamburro, L. Celotti, D. Furlan, V. Guantieri, Interaction of Pt(II) complexes with DNAs from various sources. A circular dichroism study *Chem*, Biol. Int. 16 (1977) 1–11.

[39] N. Shahabadi, L. Heidari, Synthesis, characterization and multi-spectroscopic DNA interaction studies of a new platinum complex containing the drug metformim, Spectrochim. Acta A Mol. Biomol. Spectrosc. 128 (2014) 377–385.

[40] a) J. Rajesh, M.P. Kesavan, S. Ayyanaar, K. Karthikeyan, G. Rjagopal, P. Athappan, DNA Interaction and cleavage studies of ancillary chiral ligand and *N*,*N*-donor ligands coordinated platinum(II) complexes, Appl. Organomet. Chem. 31 (2017) e3868;
b) N. Shahabadi, Z.M. Kalar, N.H. Moghadam, DNA interaction studies of platinum (II) complex containing an antiviral drug, ribavirin: the effect of metal on DNA binding, Spectrochim. Acta A Mol. Biomol. Spectrosc. 96 (2012) 723–728;
c) Q. Li, P. Yang, H. Wang, M. Guo, Diorganotin(IV) Antitumor Agent. $(C_2H_5)_2SnCl_2$(Phen)/ nucleotides aqueous and solid-state coordination chemistry and its DNA binding studies, J. Inorg. Biochem. 64 (1996) 181–195.

[41] a) A.L. Querino, K.B. Enes, O.A. Chaves, D. Ditzz, M.R.C. Couri, R. Diniz, H. Silva, Modified pyrazole platinum(II) complex can circumvent albumin and glutathione: synthesis, structure and cytotoxic activity, Bioorg. Chem. 100 (2020) 103936;
b) M. Sankarganesh, P.R.A. Jose, J.D. Raja, R.V. Solomon, C.D. Sheela, S. Gurusamy, Bioactive platinum complex of ligand bearing pyrimidine skeleton: DNA/BSA binding, molecular docking, anticancer, antioxidant and antimicrobial activities, J. Biomol. Struct. Dyn. 40 (2020) 6683–6696;
c) Q. Peña, J. Lorenzo, G. Sciortiono, S. Rodríguez-Calado, J. Maréchal, P. Bayón, A.J. Simaan, O. Iranzo, M. Capdevila, O. Palacios, Studying the reactivity of "old" Cu(II) complexes for "novel" anticancer purpose, J. Inorg. Biochem. 195 (2019) 51–60.

[42] M.J. Waring, Complex formation between ethidium bromide and nucleic acids, J. Mol. Biol. 13 (1965) 269–282.

[43] N. Shahabadi, S. Mohammadi, R. Alizadeh, DNA interaction studies of a new platinum(II) complex containing different aromatic dinitrogen ligands *Bioinorg*, Bioinorg Chem Appl. (2011). *2011*, ID 429241.

[44] B. Ray, B. Gupta, R. Mehrotra, Binding of platinum derivative, oxaliplatin to deoxyribonucleic acid: structural insight into antitumor action, J. Biomol. Struct. Dyn. 37 (2019) 3838–3847.

[45] A.N. Houghton, D. Polsky, Focus on melanoma, Cancer Cell 2 (2002) 275–278.

[46] E. De Vries, J.W. Coebergh, Cutaneous malignant melanoma in Europe *Eur*, J. Cancer 40 (2004) 2355–2366.

[47] B. Domingues, J.M. Lopes, P. Soares, H. Pópulo, Melanoma treatment in review, ImmunoTargets Ther 7 (2018) 35–49.